Award Number:
W81XWH-10-1-0732

TITLE:
Mass Scale Biosensor Threat Diagnostic for In-Theater Defense Utilization

PRINCIPAL INVESTIGATOR:

Joe Leigh Simpson, M.D.

CONTRACTING ORGANIZATION:
Florida International University

Miami, FL 33199

REPORT DATE:

October 2012

TYPE OF REPORT:
Annual

PREPARED FOR: U.S. Army Medical Research and Materiel Command
Fort Detrick, Maryland 21702-5012

DISTRIBUTION STATEMENT:

Approved for public release; distribution unlimited

REPORT DOCUMENTATION PAGE

Form Approved
OMB No. 0704-0188

1. REPORT DATE *(DD-MM-YYYY)*	**2. REPORT TYPE**	**3. DATES COVERED** *(From - To)*
1 October 2012	Annual	20 Sept 2011 - 19 Sept 2012

4. TITLE AND SUBTITLE

Mass Scale Biosensor Threat Diagnostic for In-Theater Defense Utilization

5a. CONTRACT NUMBER
W81XWH-10-1-0732

5b. GRANT NUMBER
0

5c. PROGRAM ELEMENT NUMBER

6. AUTHOR(S)
Joe Leigh Simpson, MD simpsonj@fiu.edu

Chenzhong Li, Ph.D.
Renee Martin, Ph.D.

Anthony McGoron, Ph.D.
Helen Tempest, Ph.D.

5d. PROJECT NUMBER

5e. TASK NUMBER

5f. WORK UNIT NUMBER

7. PERFORMING ORGANIZATION NAME(S) AND ADDRESS(ES)
Florida International University
11200 SW 8th Street,
Miami, Florida 33199

8. PERFORMING ORGANIZATION REPORT NUMBER

9. SPONSORING / MONITORING AGENCY NAME(S) AND ADDRESS(ES)
U.S. Army Medical Research and
Materiel Command
Fort Detrick, Maryland
21702-5012

10. SPONSOR/MONITOR'S ACRONYM(S)

11. SPONSOR/MONITOR'S REPORT NUMBER(S)

12. DISTRIBUTION / AVAILABILITY STATEMENT
Approved for public release: distribution unlimited

13. SUPPLEMENTARY NOTES

14. ABSTRACT

The goals of this project are to develop two biosensors capable of rapidly assessing exposure to unknown toxicants and to validate these biosensors by "gold-standard" cytogenetic assays. We have made significant progress in all three areas of the project. 1) Cytogenetics: Dose responses have been validated for UV and H202 for all three cytogenetic assays with increasing levels of DNA damage observed with increasing exposure to genotoxic agents. 2) EIST biosensor: We have successfully established a calibration method for quantitative analysis of 8-OHdG colorimetric testing in standard solution, diluted urine and cell culture medium. In addition, we have successfully integrated the Carbon nanotube (CNT) paper electrode to the paper strip based platform, and tested the 8-OHdG concentrations by traditional colorimetric method as well as electrochemical method. 3) Gold nanoparticle whole-cell based biosensor: we have demonstrated the proof-of-concept that silver, and possibly gold, are suitable SERS substrates for selective and specific detection of Hsp70 and RAD54 proteins from yeast exposed to environmental stress, but have not yet been able to load sufficient quantities of the SERS sensors into the yeast cells to measure the proteins intracellularly. During the next year we will assess the accuracy and reliability of these 2 biosensors

15. SUBJECT TERMS
Biosensors to detect exposure to unspecified toxicants
Gold nanoparticles and Raman spectroscopy
Validation of cytogenetic gold standard assays
Reactive oxidative DNA damage and 8-OHdeoxyguanosine

16. SECURITY CLASSIFICATION OF:			**17. LIMITATION OF ABSTRACT**	**18. NUMBER OF PAGES**	**19a. NAME OF RESPONSIBLE PERSON**
a. REPORT	**b. ABSTRACT**	**c. THIS PAGE**			USAMRMC
U	U	U	UU	55	**19b. TELEPHONE NUMBER** *(include area code)*

Contents Page

1. General Introduction

Currently there is no practical or rapid method to monitor exposures to biological weapons of unknown nature, either chemicals or pathogens on the battlefield or chemicals encountered during environmental cleanup programs. Need is especially acute for assessing exposures to unspecified toxicants, i.e., agents unknown at time of exposure. If the toxic agent were known, a specific assay could be readily developed, and indeed many options already exist to detect specific toxicants. If the toxic agent is not known or suspected, a different approach is necessary to monitor the exposure to toxicity. Inexpensive assays must be developed that provide rapid assessment and warn of toxicity in the environment (e.g., in water and air) and personnel exposure. This could then be followed by more detailed and expensive laboratory analysis to identify the specific toxicant. Sorely needed is a device comparable to the familiar dosimeter "badge", which determines cumulative radiation exposures. The current approach for assessing radiation and genome toxicity relies principally on scoring for chromosomal abnormalities. These measures of genotoxicity are currently only possible through laborious cytogenetic evaluations requiring dedicated lab personnel with extensive training.

No biomedical devices can identify exposures to toxicants sensitively and in "real-time" fashion. Thus, at the present time, cytogenetic methods remain the "gold-standard", but "rapid" user-friendly (i.e., less labor intensive) and cost-effective methods are desired. The goals of this project are to develop two biosensors (i) EIST biosensor measuring reactive oxygen species specifically 8-OHdG; and (ii) SERS biosensor measuring several stress proteins. Each should be capable of rapidly assessing exposure to toxicants that are unknown or unspecified and validated by proven cytogenetic assays.

1.1. Gold-Standard Cytogenetic Assays Background

Assessments of the effects of chemical and physical agents on DNA have been made using a variety of genotoxicity and mutagenicity assays. Unfortunately, the numerous mechanisms through which different genotoxic agents can act dictate that no single test can detect all forms of DNA damage. Testing requires a multifaceted approach. Standard cytogenetic assays used for comparison in this project represent the "industry gold-standard" assays for genotoxicity and biomonitoring testing: Chromosome Aberration (CA); Micronuclei assay (MN); and Comet assays.

Clastogenic and aneugenic agents have been shown to result in a biologically significant increase in the frequency of cells with structural or numerical chromosomal aberrations. The CA assay detects both numerical and structural aberrations. The MN assay counts small extranuclear bodies that are formed during mitosis as a result of chromosome breaks or interference in the mitotic process, resulting in lagging chromosome(s) that lead to formation of MN (Sari-Minodier et al., 2007). The Comet assay measures DNA damage resulting from single- and double-stranded breaks. Undamaged DNA retains its highly organized association with matrix proteins in the nucleus. When damaged, however, this organization is disrupted; DNA fragments disperse and migrate out of the cell nuclei (Glei et al., 2009).

1.2. Biosensor 1 Background: EIST Based Biomarker Sensor For Oxidative DNA Damage Assessment

Numerous agents of biological and chemical warfare (Kang et al., 2006 Kuhn et al., 2006) induce oxidative damage in cells. 8-OHdG is the most commonly studied biomarker for cellular oxidative stress, DNA damage and repair mechanisms. Upon oxidation, a hydroxyl free radical attack arises at the C-8 position of deoxyguanosine in DNA, resulting in production of 8-Hydroxy-2-deoxyguanosine (8-OHdG) (Kasai et al., 1984). Urinary 8-OHdG is commonly measured in the laboratory setting; elevated urinary 8-OHdG concentrations are associated with environmental exposures including chemical toxins (Erhola et al., 1997) and radiation (Sperati et al., 1999). Levels of 8-OHdG are expected to be proportional to the cumulative toxicity levels of many toxicants and their duration of exposure. Periodic monitoring of 8-OHdG levels in personnel working at military installations and battlefield sites could thus enable assessment of unspecified toxicant exposure to various biological, chemical and radiation warfare agents. Here we will develop a simple competitive colloidal gold-based electrochemical immunoassay in lateral-flow format for the rapid detection of 8-OHdG. Nitrocellulose membrane strip is separately coated with goat anti-mouse IgG (control line) and 8-hydroxyguanosine-BSA conjugate (test line) (Figure 1). Initially anti-8-Hydroxyguanosine (8-OHG) monoclonal is labeled with gold nanoparticles. Using both standards and spiked urine solutions, a positive reaction results in the remaining antibody-gold conjugate combining with antigen coated on the membrane for obvious visual detection. Further, electrochemical capacity will be integrated into the same system to give better quantitative information. The test strip will thus provide a point-of-care testing method for quantitative, semi-quantitative, or qualitative detection of DNA oxidative stress with high sensitivity, specificity, speed of performance and the advantages of simplicity.

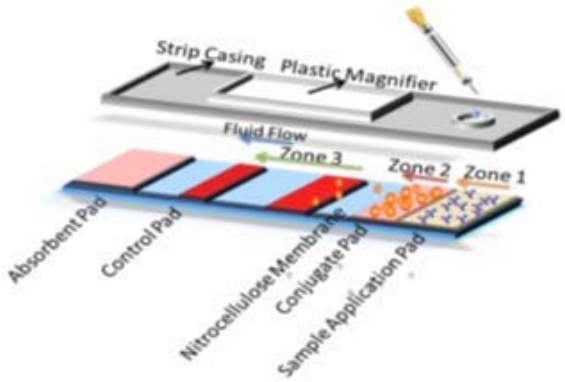

Figure 1. Schematic illustration of the lateral flow strip for 8-OHdG biomarker detection. Upon competitive type assays, the Au particles labeled by anti-8-OHdG antibody flow along a thin solid matrix together with the analytes driven by capillary force and eventually accumulate upon immune recognition at a defined area pretreated by antibody or antigen. Qualitative or semi-quantitative detection of various analytes is thus realized by colorimetry read either by naked eyes or with the aid of optical density analysis.

1.3. Biosensor 2 Background: SERS Based Gold Nanoparticle Whole-Cell Biosensor

Raman spectroscopy identifies chemicals structures based on the inelastic scattering of light by the vibrational modes of chemical bonds of molecules. Scattering of a laser light from a protein produces a spectrum of Raman peaks, each characteristic of a specific vibration of a molecular bond. However Raman spectroscopy has a relatively low molecular cross-section (Aroca et al., 2006). Surface Enhanced Raman Spectroscopy (SERS) overcomes this limitation in enhancing the Raman signal when the analyte

is in close proximity to the metal. (Nie et al., 1997). Metal nanoparticle such as silver, gold, copper, and platinum are finding large applications in chemical and biological sensing.

Response of yeast to stress is well known (Magar et al., 1993) and utilizing yeast cells as an surrogate for whole cell sensor development has several advantages i) they are eukaryotic and robust; ii) and they can not be dried at 28-40^{o}C, stored for more than a year, and be immobilized in various substrate including membranes and gel until needed. This robust nature of yeast cells can be easily exploited to monitor the exposure to stress by having a method to quantify the response (expression of proteins) of yeast to stress.

Label-free detection and identification of proteins by SERS, has been well documented in the literature (Li et al., 2006). Specific proteins in cellular matrices and the intracellular environment can be detected based on a protein-protein (antibody-antigen) interaction using SERS. In this aspect, gold nanoparticles with optimal size around 30nm have been very much utilized to detect protein interactions. Combined with the ability for qualitative assessment, the quantitative measurement ability using SERS to detect a wide range of molecules simultaneously makes the SERS sensors versatile.

To measure the expressed stress proteins (Hsp70, RAD54 and Caspase-3), antibody tagged gold nanoparticles can be delivered into yeast cells followed by measurement of the yeast response to stress such as UV, H_2O_2 and others non-invasively using SERS. The sensor development will involve aspects of Gold nanoparticle synthesis, linker attachment, antibody binding, nanoparticle uptake and detection of proteins both outside (in cell lysate) and within yeast cells (Figure 2), device fabrication and determination of the sensitivity in the measurement of stress proteins using existing conventional technique (ELISA or Western-blot).

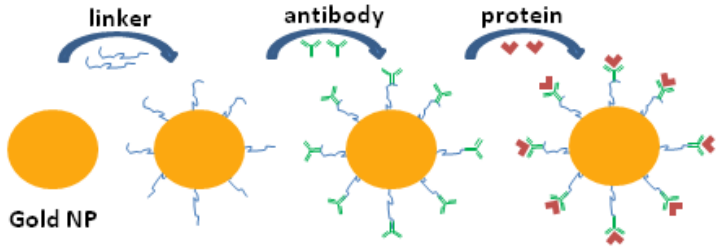

Figure 2 Schematic of the Gold or Silver nanoparticle SERS sensor. The presence of the protein conjugated to gold nanoparticle-antibody complex will be detectable by SERS

2. Body

2.1. Cytogenetic Assays

OVERALL PROJECT OBJECTIVES: To establish and validate "gold-standard" cytogenetic assays CA, MN and the Comet assay, using standardized genotoxic agents H_2O_2 and UV to measure DNA damage in human lymphocytes in-vitro.

2.1.1. IRB Approval

The cytogenetics component of the "mass scale biosensor threat diagnostic for in-theater defense utilization" project required approval by both Florida International University (FIU) and the Telemedicine and Advanced Technology Research Center [TATRC] institutional review boards (IRB). The IRB protocol details the procedure that is followed. In brief: Healthy volunteers wishing to participate in this research study donate approximately 10ml of blood to be collected by venipuncture at the FIU University Health Center. Donors must be aged 18 to 70-years-old and are required to complete a short lifestyle questionnaire determining any prior genotoxic exposure. Donors may be excluded from participating if they are deemed "unhealthy" on the basis of their responses on the questionnaire. Blood samples are de-identified and coded with a project number. Multiple blood cultures are established from blood collected from the research participants. These are cultured (in-vitro) in the presence of genotoxic agents (ultra-violet [UV] light and hydrogen peroxide [H_2O_2]). UV and H_2O_2 have been selected as genotoxic agents in this project since both have well defined mechanisms of action and are frequently utilized as positive controls "standardized" agents in DNA damage assays. Blood samples are cultured in the presence of these agents at increasing concentrations of H_2O_2 and increasing duration of exposure to UV to establish a dose-effect relationship. The IRB protocol was approved 03/28/2011, A deviation was submitted because compensation procedures listed on the protocol were not followed. According to the protocol, the phlebotomist would store and distribute a $16 gift card. Due to mandatory procedures from a financial perspective, the administrative assistance not part of the research team stored and provided gift cards to research participants. An amendment was submitted updating the compensation procedure.

2.1.2. Research Participant Recruitment

In conjunction with the FIU University Health Center, guidelines were established at the outset of the project along with a standard operating protocol that was submitted as part of the supporting documents for the IRB process. Since the last annual report we have recruited an additional 44 healthy volunteers bringing the total number of subjects partaking in this project to a total of 53 (14 males and 39 females). To date, we have encountered no difficulties in recruiting volunteers and no adverse events have been reported.

2.1.3. Blood Cultures

In order to be able to perform the CA and MN assays, human lymphocytes collected by venipuncture must be cultured and stimulated to enter cell division. The reason for this is twofold. First, the CA assay requires cells to be in a specific stage of cell division (metaphase) in order that the DNA is condensed, thus allowing identification of individual chromosomes based on size, centromere position and banding pattern after staining. Second, mammalian cells have a battery of repair mechanisms in their arsenal to correct DNA damage. This can be accomplished at various points as cells progress through the cell cycle. The end result of the induction of DNA damage and the various repair mechanisms available includes: (i) DNA damage can be repaired, resulting in DNA that is no longer altered; (ii) the cell is damaged beyond repair and initiates apoptosis (cell death). Apoptosis is initiated when a cell is unable to proceed past

various cell cycle checkpoints, largely in place to recognize the presence of multiple/harmful unrepaired DNA damage; (iii) DNA damage is unsuccessfully recognized and/or repaired, but the cell evades apoptosis and manages to progress through the cell cycle. For the purposes of this project we are largely interested in points ii) and iii), primarily because the scenario listed in i) indicates that the DNA damage is minimal and passes unrecognized within the cell. Pathways ii) and iii) are clearly detrimental, apoptosis of large numbers of cells due to excessive DNA damage being potentially disastrous. Of more concern is DNA damage capable of evading DNA damage recognition and/or repair persisting in the cell such that future generations of the cell continue to divide. In this situation the DNA damage can be passed to future daughter cells, and depending on the type of damage and location within the genome, could result in diseases such as cancer. Therefore, we have focused our attention on exposing lymphocytes to genotoxic agents in-vitro but allowing cells to divide in culture. We can thus analyze DNA damage that has evaded DNA repair mechanisms and cell cycle check-points to persist. The comet assays requires that lymphocytes are isolated exposed and processed for analysis the same day.

Our laboratory has established the requisite parameters to optimize the culturing of human lymphocytes. These are largely the same for all three DNA damage assays (CA, MN and Comet). The only significant difference between the assays is that the comet assay is processed within 24 hours versus 72 hours for the CA and MN. Specifically, we have performed experiments to determine the culture conditions, appropriate culture media and various chromosome preparation methods to obtain a high yield of cell division and high quality metaphases for the CA assay. As per standardized guidelines for genotoxic assays, the mitotic index for each culture must be monitored. This measure of the proliferation status of a cell population is defined as the ratio between the number of cells in mitosis and the total number of cells. The maximum concentration of a genotoxic agent must not surpass a reduction of more than 50% cell proliferation compared to unexposed cell cultures (indicative of excessive amounts of DNA damage) for the CA assay. The MN assay utilizes a cytokinesis-block proliferation index (CBPI) to evaluate the effect of cytotoxicity and cell proliferation. For the comet assay no measurement of cell proliferation is performed, however, cell apoptosis is noted to evaluate genotoxic exposure.

2.1.4. Dose-Responses

Range-finding experiments for in-vitro H_2O_2 and UV exposure to induce DNA damage in lymphocytes have been established for each of the three assays. The different assays are based on evaluating different types of DNA damage and hence the sensitivity of these assays require some differences in concentration and exposure times in order to induce measurable DNA damage (Tables 1 and 2) without a significant reduction in cell proliferation or induction of massive cell death (apoptosis). For each assay CA, MN and comet the lymphocytes are exposed for a set duration and then cultured with media not containing the genotoxic agent for several hours (comet assay) or 72 hours (CA and MN assay)

To date, we have tested concentrations of H_2O_2 in the range of 0-80mM and 0-30 minutes exposure to UV (dependent on the assays being tested) (Tables 1 and 2); this range was chosen initially based on pre-existing published data that have traditionally utilized H_2O_2 and UV as a positive control in various genotoxic assays. Initially, blood is drawn into lithium-heparin tubes to prevent clotting, and then

aliquoted (500µl) into tubes with 9.5ml of RPMI culture media (Invitrogen, USA) to which the H_2O_2 is added to the desired final concentration or the culture is exposed to UV (range 0.25mM-80mM; 30-seconds - 30 minutes respectively). With increasing exposure to the genotoxic agents cell lysis was observed within the culture media (Figure 3). Blood cultures are set up in duplicate or triplicate depending on the DNA damage assay. Extended culture in the absence of the genotoxic agent, allows DNA repair mechanisms and cell cycle checkpoints to be initiated. Lymphocytes are then cultured for 72 hours to allow repair of DNA damage, apoptosis and progression of cell division (with or without DNA damage) (with the exception of the comet assay – processed on the same day). For the CA assay colcemid is added to the cultures at 71 hours. To disrupt the microtubule formation necessary for cells to proceed through metaphase and complete their cell cycle. Colcemid is added to arrest those cells in metaphase ensuring we have a population of cells at the desired stage of the cell cycle (metaphase) for the CA assay. Lymphocytes are subsequently centrifuged, separated from the culture media and processed through hypotonic and fixation steps. For the MN assay Cytochalasin B is added at 24 hours and left to in culture for a further 48 hours. The addition of Cytochalasin B prevents the cells from completing cytokinesis resulting in the formation of multinucleated cells. The comet assay does not require any steps to arrest cells in mitotic cell division.

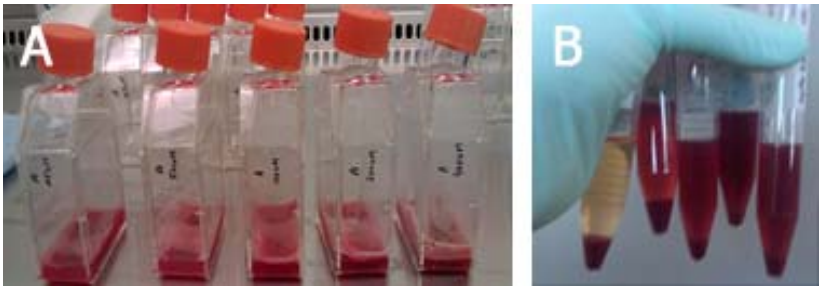

Figure 3 A) demonstrates increased cell lysis after addition of H_2O_2 (note increasing lysis (foam) increasing concentration from left-right. B) shows increasing lysis of cells after UV exposure (left control- right increasing UV exposure) visualized as darker red cell- culture media

Table 1 detailing the concentration of H_2O_2 treatment and duration of exposure for each of the three cytogenetic assays

Technique	Treatment	Concentration (mM)	Exposure duration (minutes)
Chromosome aberration assay	H_2O_2	0, 5, 10, 20, 40, 80	30
Micronuclei assay	H_2O_2	0, 0.25, 0.5, 1.0	10
Comet assay	H_2O_2	0, 0.25, 0.5, 1.0	10

Table 2 detailing the UV treatment and duration of exposure for each of the three cytogenetic assays

Technique	Treatment	Exposure duration (minutes)
Chromosome aberration assay	UVB (280-320nm)	0, 5, 10, 15, 30
Micronuclei assay	UVB (280-320nm)	0, 2, 5, 7 and 0, 1, 2, 4
Comet assay	UVB (280-320nm)	0, 2, 5, 10

2.1.5. Chromosome Aberration Assay

Processed lymphocyte cultures as outlined above are placed on glass slides. Their mitotic index is calculated for the control (unexposed) and for each exposure concentration of the genotoxic agents H_2O_2 and UV (Tables 1 and 2); each sample is replicated. The mitotic index is a ratio of the number of cells in metaphase divided by the number of cells in interphase. For both H_2O_2 and UV we observe a reduction in mitotic index with increasing concentration H_2O_2 and exposure to UV (Tables 3 and 4).

Table 3 Average mitotic index for H_2O_2 exposed lymphocytes in nine subjects

	0mM H_2O_2	5mM H_2O_2	10mM H_2O_2	20mM H_2O_2	40mM H_2O_2	80mM H_2O_2
Mitotic Index	0.0123	0.0088	0.0076	0.0060	0.0057	0.0043
Std. Dev.	0.0107	0.0090	0.0059	0.0047	0.0042	0.0034

Table 4 Average mitotic index for UV exposed lymphocytes in six subjects

	0 minutes	5 minutes	10 minutes	15 minutes	30 minutes
Mitotic Index	0.0175	0.0060	0.0075	0.0045	0.0035
Std. Dev.	0.0064	0.0021	0.0060	0.0066	0.0012

Slides are subsequently stained with 4',6-diamidino-2-phenylindole (DAPI) to permit analysis of chromosomes for the CA assay, using reverse DAPI banding. Metaphase spreads are visualized and captured using an Olympus BX61 fluorescence microscope at a magnification of x1000 with Smart Capture image analysis software (Digital Scientific, UK). Captured images are then imported into the karyotyping software SmartType (Digital Scientific, UK), which enables the operator to isolate individual chromosomes and classify each chromosome on the basis of size, centromere position and banding pattern (Figure 4).

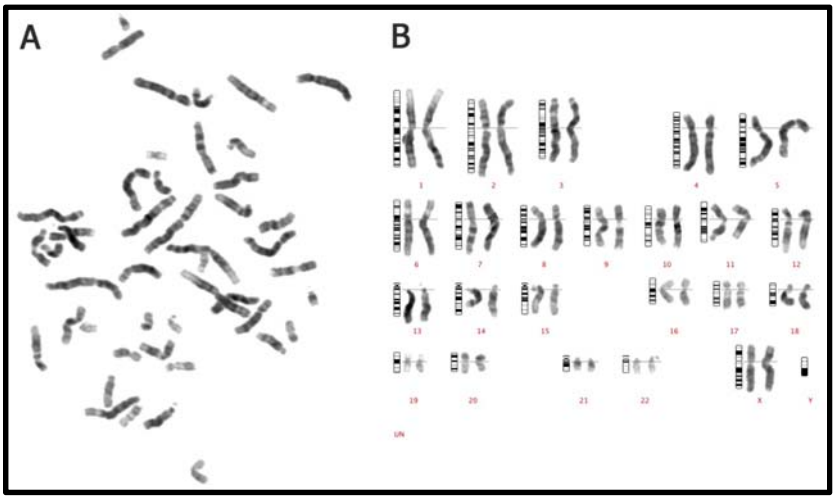

Figure 4: A) Reverse DAPI banded chromosome metaphase spread, illustrating how chromosomes can be visualized after staining with DAPI and identified by characteristic banding patterns, chromosome size and centromere position. B) A normal 46,XX female karyotype. This demonstrates how chromosomes (taken from Figure 1A) can be isolated, identified and aligned. G-band ideograms (schematic representation of the banding patterns) are located to the left of each chromosome pair. Chromosome number is indicated beneath the respective

When possible a minimum of 50 metaphases are analyzed per sample per concentration of genotoxic agent.

To date, our analysis of cultured lymphocytes from individuals not exposed to any genotoxic agent (all 25 study participants) showed a normal human karyotype (normal chromosomes). Multiple attempts were made to establish the most appropriate concentration and exposure times of the genotoxic agents, the finalized concentrations and exposures are presented in Tables 1 and 2. To date we have performed experiments in 15 subjects (nine for H_2O_2 and six for UV). Of these analysis has been completed in eight subjects for H_2O_2 and two for UV, the remaining are in the process of analysis. Lymphocytes from all these subjects showed chromosome aberrations deemed by the CA assay to be the result of exposure to the genotoxic agent H_2O_2 or UV.

The CA assay enables identification of chromosomal aberrations (e.g., deletions, duplications, translocations, fragile sites and inversions) that are at least 5 megabases (Mb) in size. Specific observations include a reduction in cell proliferation (Tables 3 and 4) and an increase in cell lysis with increasing H_2O_2 concentration and UV exposure (Figure 3). In addition, we have been able to observe abnormalities at all concentrations and exposures tested, their frequency and severity increasing with higher concentrations (Figures 13-16). The results for each subject detailing the aberrations observed at the different concentrations and exposures can be found in Tables 5-12.

Hydrogen peroxide chromosome aberration assay results

These results are presented for each subject. An example of a normal karyotype from each individual is presented in Figures 5-11 and details of the chromosome aberrations identified for each of the tested concentrations are provided for each subject in Tables 5-11

Figure 5 Normal metaphase and karyotype from control sample subject #6

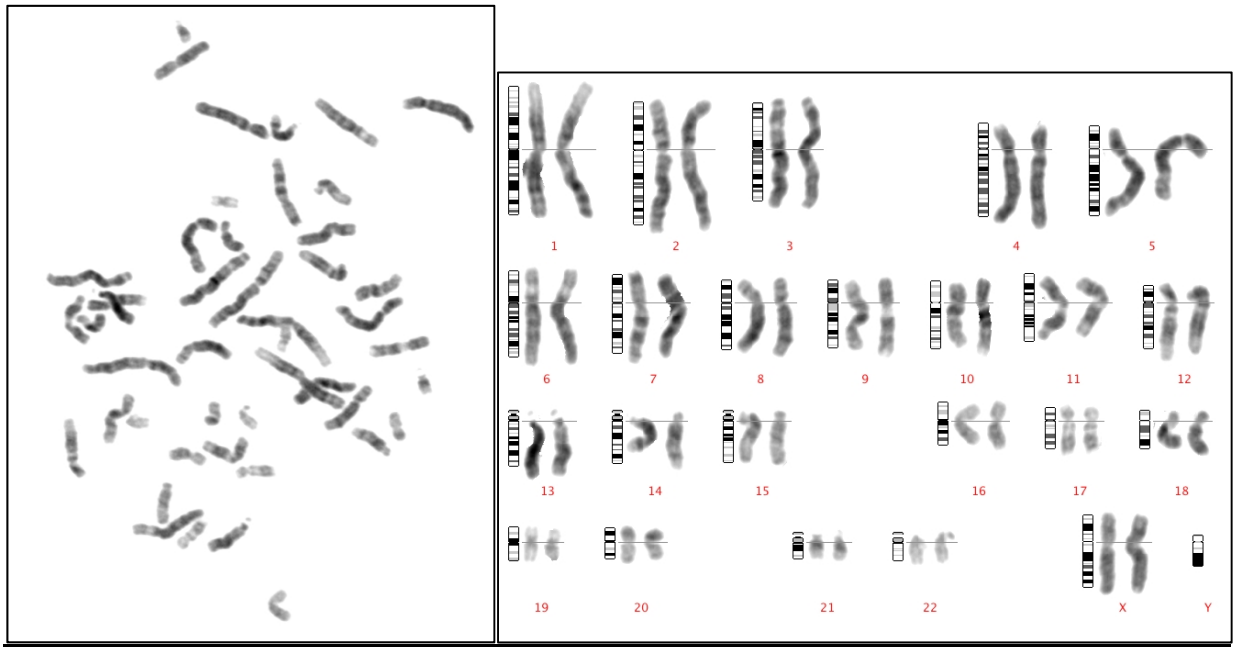

Table 5 Chromosome aberrations observed after exposure to H_2O_2 in subject #6

H_2O_2 treatment	No of cells analyzed	Chromosome aberrations observed (#) indicate multiple cells with aberration	Aberration symbol
5mM	38	Chromatid deletion on chromosome 4q with the loss of segments 4q31 to 4q35	cht del(4)(q31q35)
		Chromosome break on chromosome 8 at band 8q21	chrb(8)(q21)
		Distorted appearance of chromosomes (Abnormal cell representing the damaged metaphase)	pvz
		Marker chromosome	42, XX,-6,-15,-19,-22,+mar
10mM	49	Distorted appearance of chromosomes (3)	pvz
		Premature centromere division	pcd
		Tri-Satellite associations between the 'DGG' group chromosomes	
		Di-Satellite associations between the 'DD' and `DG' group chromosomes (2)	
20mM	40	Deletion of the long arm of chromosome 5, but unclear whether it is a terminal or an interstitial deletion	[46,XX,del(5)(q34-qter)?? or 46,XX,del(5)(q34)??]
		Premature centromere division noted in many chromosomes	pcd
40M	53	Premature centromere division noted in many chromosomes resulting in many fragments	pcd
		Distorted appearance of chromosomes (Many abnormal cells representing the damaged metaphases)	pvz
80mM	45	Distorted appearance of chromosomes	pvz
		Premature centromere division	pcd
		Chromatid break in chromosome at band 10q22	cht(10)(q22)
		Chromosomes noted with multiple gaps and distorted morphology	
		Di-Satellite associations between the 'DG' and `GG' group chromosomes	

Figure 6 Normal metaphase and karyotype from control sample subject #10

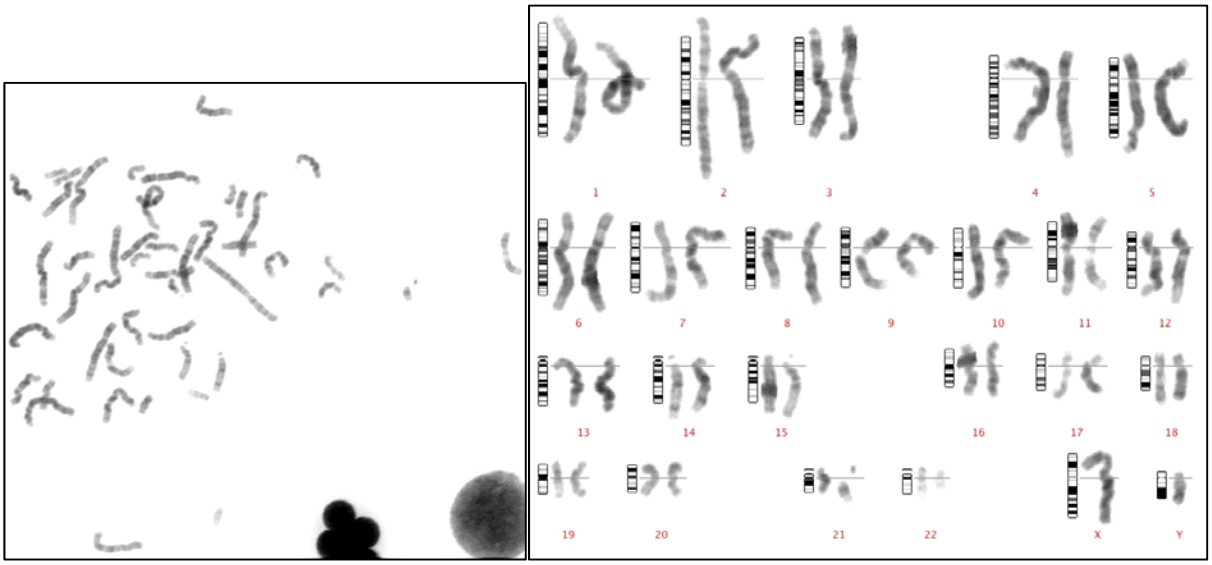

Table 6 Chromosome aberrations observed after exposure to H_2O_2 in subject #10

H_2O_2 treatment	No of cells analyzed	Chromosome aberrations observed (#) indicate multiple cells with aberration	Aberration symbol
5mM	50 cells	Dicentric chromosomes 3p and 7q	
		Dicentric chromosomes 2q and 8q	
		Chromosome break in chromosome 1 at band 1p35	chrb(1)(p35)
		Chromsome gap in chromosome 13 at band 13q21	chrg(13)(q21)
		Acentric fragment	ace
		Chromosome break in chromosome 1 at band 1p36.1	chrb(1)(p36.1)
		Dicentric chromosome 6p and satellite associations between the 'D' group chromosomes; acrocentric chromosome association involving chromosomes 13 and 14 respectively.	
		Premature chromosome division generating many fragments	pcd
		Satellite associations between the 'DG' group chromosomes; acrocentric chromosome association involving chromosomes 14 and 21 respectively (2).	
10mM	50 cells	Chromosome break in chromosome 12 at band 12q24.2	chrb(12)(p24.2)
		Acentric fragment	ace
		Rearranged metaphase chromosome showing a triradial configuration; three arms to the pattern and several chromosomes with distorted appearance	
		Distorted appearance of chromosomes (3)	pvz
20mM	50 cells	Tetroploid metaphase and chromosome gap in chromosome 3	
		Distorted appearance of chromosomes	pvz
		Acrocentric chromosome associations (2)	
		Premature chromosome division generating many fragments	pcd
40mM	50 cells	Chromosome break in chromosome 5 at band 5q34	chrb(5)(p34)
		Premature chromosome division	pcd
		Distorted appearance of chromosomes	pvz
		Acrocentric chromosome associations (2)	
80mM	50cells	Two chromatic breaks in a single metaphase on chromosome 5q and chromosome Xq	chtb(5)(q32) chtb(X)(q21)
		Distorted appearance of chromosomes	pvz

Figure 7 Normal metaphase and karyotype from control sample subject #30

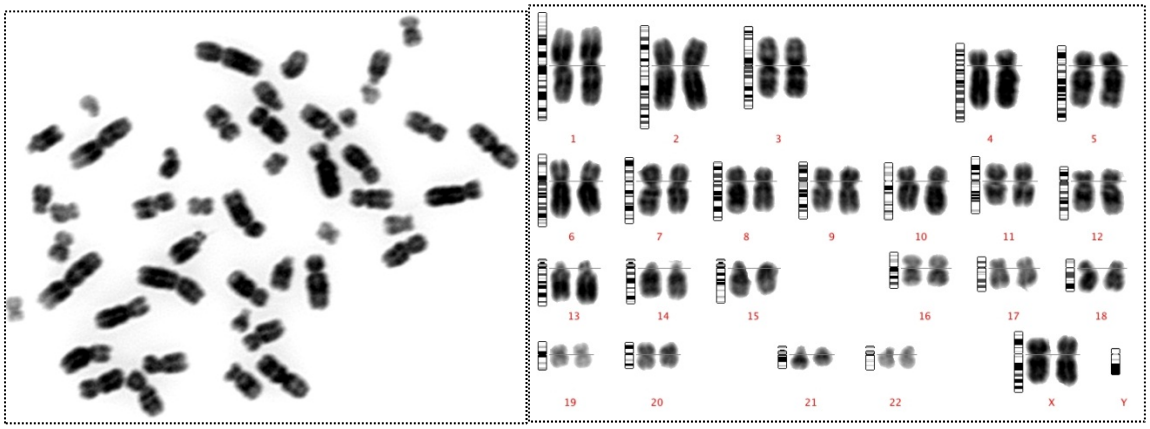

Table 7 Chromosome aberrations observed after exposure to H_2O_2 in subject #30

H_2O_2 treatment	No of cells analyzed	Chromosome aberrations observed (#) indicate multiple cells with aberration	Aberration symbol
0mM	50 cells	Acentric fragment	ace
		Premature chromosome condensation seen as chromatin of S-phase nuclei appears to be pulverized	pcc/pvz
5mM	50 cells	Distorted morphology	pvz
		Chromatid breaks in chromosomes 4 at band 4q25 and chromosome X at band Xq26	chtb (4)(q25) chtb (X)(q26)
		Acrocentric association involving D and G chromosomes that include chromosomes 13 and 21. (x2)	
10mM	50 cells	Chromatid break in chromosome 10 at band 10q23	chtb (10)(q23)
		Distorted appearance of chromosomes	pvz
		Association between the telomeric regions of the long arm of chromosome 10 and short arm of chromosome 22	tas(10;22)(q26;p13)
20mM	50 cells	Distorted appearance of chromosomes (x3)	pvz
40mM	50 cells	Extra chromosomal material/additional material on chromosome 22	add(22)(p21)
		Chromatid break in chromosome 3 at band 3p21	chtb (3)(p21)
		Acrocentric chromosome associations (x2)	
80mM	50cells	Chromatid break in chromosome 18 at band 18q21	chtb (18)(q21)
		Tri-acrocentric association involving chromosomes from DGG group, includes chromosomes 21, 22 and 13.	
		Chromatid break in chromosome 3 at band 3p21	chtb (3)(p21)
		Dicentric chromosome 1q	dic(1)(q41)
		Distorted appearance of chromosomes	pvz

Figure 8 Normal metaphase and karyotype from control sample subject #32

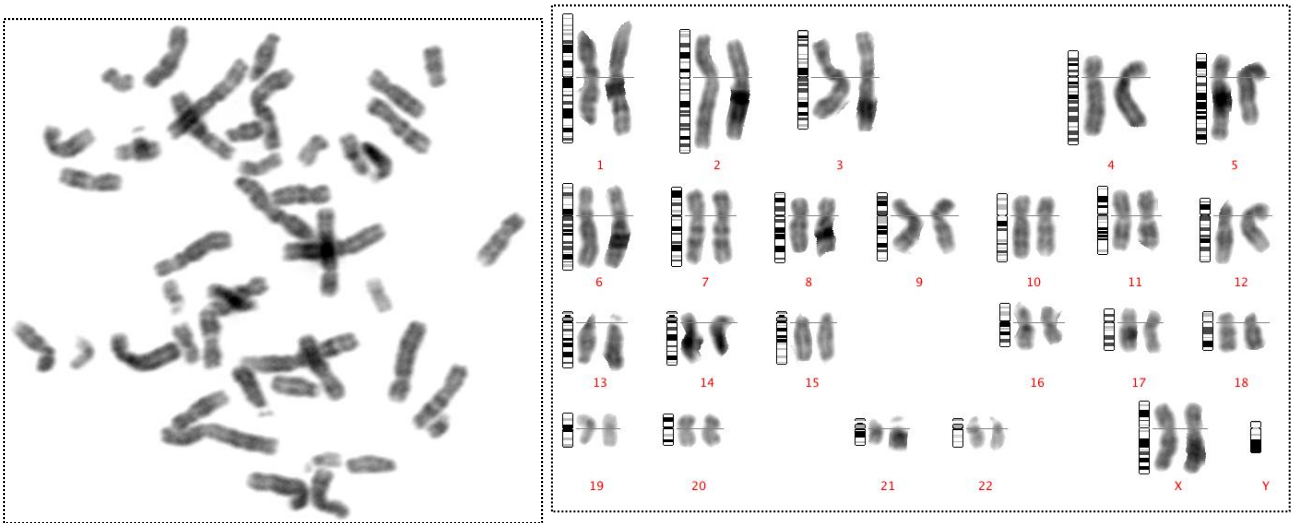

Table 8 Chromosome aberrations observed after exposure to H_2O_2 in subject #32

H_2O_2 treatment	No of cells analyzed	Chromosome aberrations observed (#) indicate multiple cells with aberration	Aberration symbol
5mM	50 cells	Distorted morphology	pvz
		Chromatid break in chromosome X at band Xq23	chtb (X)(q23)
		Chromosome break in chromosome 12 at band 12p12	chrb (12)(p12)
10mM	50 cells	Robertsonian translocation involving chromosome 6 and an unidentified chromosome	rob, (6;?)(q27;?)
		Chromosome break in chromosome 3 at band 3p21	chrb (3)(p21)
20mM	50 cells	Distorted appearance of chromosomes	pvz
		Acrocentric association involving chromosomes from DG group that include chromosomes 13 and 21	
		Metaphase with multiple chromosome rearrangements: Break in chromosome 2, dicentric chromosome 6 and terminal break in chromosome X	
40mM	50 cells	Premature centromere division	pcd
		Distorted appearance of chromosomes	pvz
80mM	50cells	Gap in chromosome 2 at band 2q23	chrg (2)(q23)
		Break in chromosome 1 at band 1p36	chrb (1)(p36)
		Acentric fragment	ace
		Acrocentric association involving chromosomes from DG group that include chromosomes 13 and 21	
		Break in chromosome 2 at band 2q21	chrb (2)(q21)
		Chromatid break in chromosome 7 at band 7q22	chtb (7)(q22)

Figure 9 Normal metaphase and karyotype from control sample subject #33

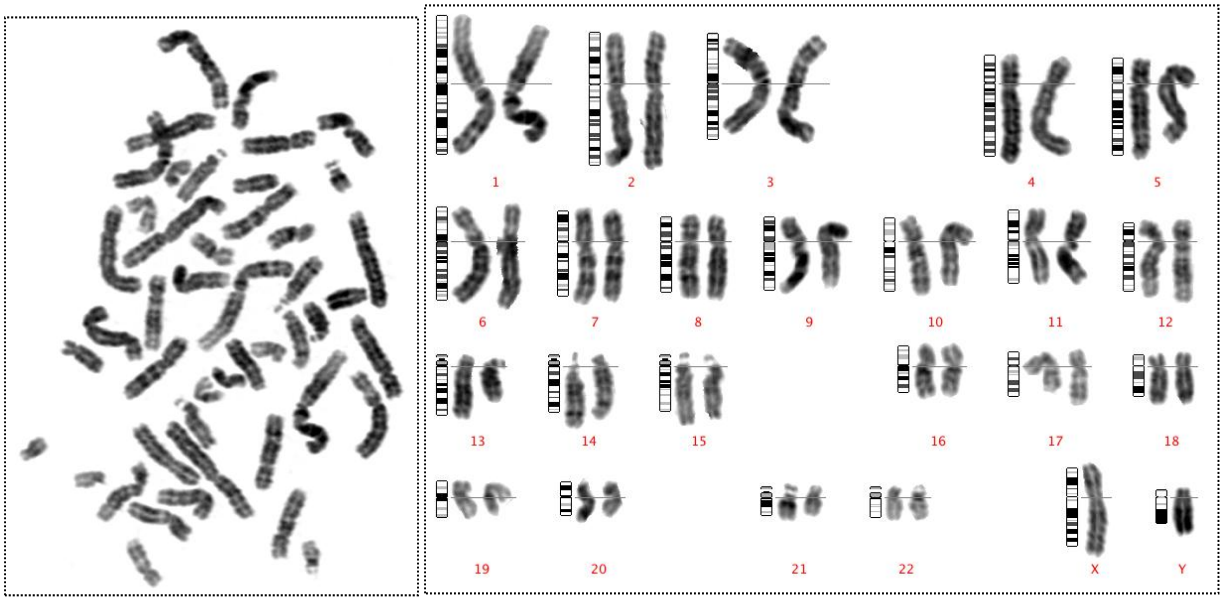

Table 9 Chromosome aberrations observed after exposure to H_2O_2 in subject #33

H_2O_2 treatment	No of cells analyzed	Chromosome aberrations observed (#) indicate multiple cells with aberration	Aberration symbol
Controls	50 cells	Distorted morphology	pvz
		Chromosome showing a triradial configuration-three arms to the pattern in chromosome 2	
5mM	30 cells	Distorted morphology (x2)	pvz
		Chromatid break in chromosome 1 at band 1q34	chtb(1)(q42)
		Chromatid break in chromosome 14 at band 14q31	chtb(14)(q31)
		Acrocentric chromosome associations involving chromosomes 14 and 21	
10mM	30 cells	Acentric fragment	ace
		Acrocentric chromosome associations involving chromosomes 14 and 15	
20mM	23 cells	Distorted appearance of chromosomes	pvz
40mM	39 cells	Acrocentric chromosome associations involving chromosomes 14, 15 and 21 and chromosomes 13 and 15	
		Acrocentric chromosome associations involving homologous chromosomes 14	
		Distorted morphology	pvz
		Break in chromosome 12 at band 12p12	chrb(12)(p12)
80mM	22cells	Acrocentric chromosome associations involving chromosomes 14 and 21	
		Premature centromere division	pcd

Figure 10 Normal metaphase and karyotype from control sample subject #34

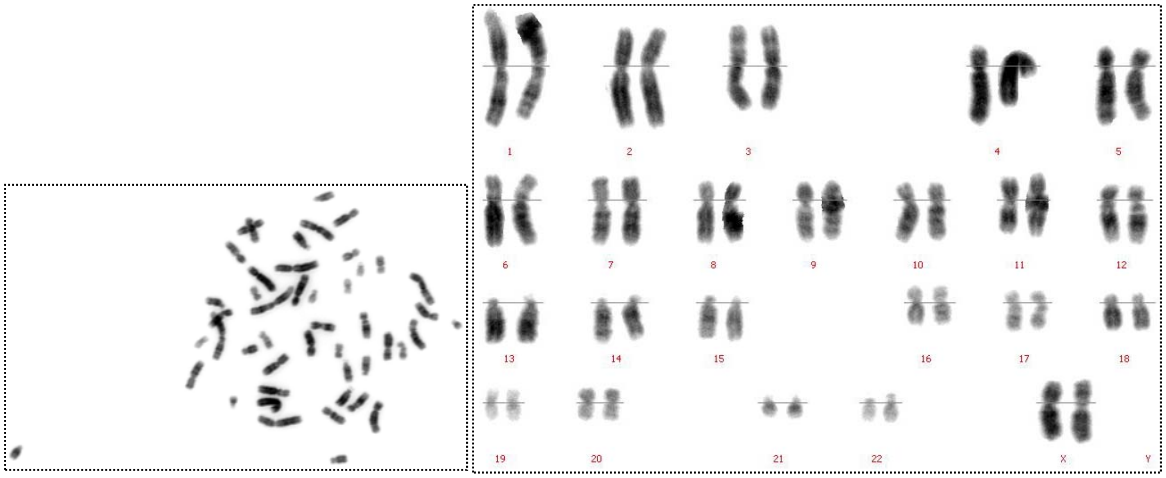

Table 10 Chromosome aberrations observed after exposure to H_2O_2 in subject #34

H_2O_2 treatment	No of cells analyzed	Chromosome aberrations observed (#) indicate multiple cells with aberration	Aberration symbol
Controls	50 cells	Distorted morphology	pvz
5mM	50 cells	Distorted morphology	pvz
		Acrocentric chromosome associations involving chromosomes 14 and 21	
		Chromosome break at band 3q21 (x3)	chrb(3)(q21)
		Chromosome break at band 9q12 (x2)	chrb(9)(q12)
		Marker chromosome with a break	mar
10mM	50 cells	Deletion of q arm in chromosome 16	del (16)(q11.2->qter)
		acrocentric chromosome associations involving chromosomes 14 and 22	
		Distorted morphology	pvz
		Acrocentric chromosome associations involving chromosomes 14 and 15 Deletion of q arm in chromosome 9 Gap in chromosome 6	del (9)(q12->qter) chrg (6)(q23)
20mM	50 cells	Distorted appearance of chromosomes (x3)	pvz
		Chromosome break at band 9p21	chrb(9)(21)
		Ring chromosome ?	r
40mM	50 cells	Distorted morphology	pvz
		Chromosome break at band 6p22	chrb(6)(p22)
80mM	50 cells	Chromosome break at band 3p21	chrb(3)(p21)
		Distorted morphology	pvz

Figure 11 Normal metaphase and karyotype from control sample subject #39

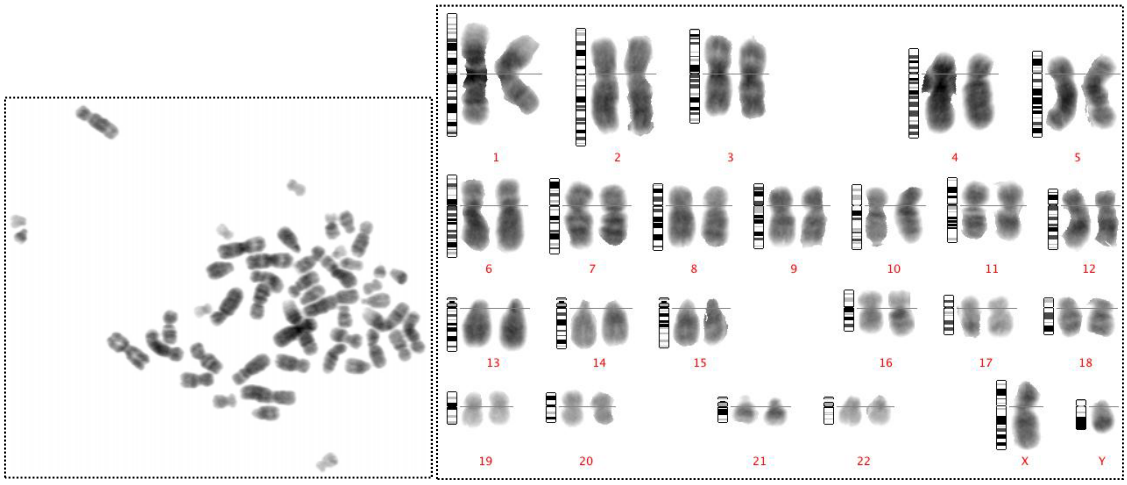

Table 11 Chromosome aberrations observed after exposure to H_2O_2 in subject #39

H_2O_2 treatment	No of cells analyzed	Chromosome aberrations observed (#) indicate multiple cells with aberration	Aberration symbol
5mM	50 cells	Distorted morphology (x3)	pvz
		Chromosomes with multiple gaps and distorted morphology	
		Break in chromosome 1 at band 1q42	chrb (1)(q42)
		Tri-Satellite associations between the 'DGG' group chromosomes; acrocentric chromosome associations involving chromosomes 14 and both 21 chromosomes.	
		Di-Satellite associations between the 'DD', DG and GG group chromosomes	
10mM	50 cells	Chromosome break at band 18q21	chrb(18)(21)
		Chromosome break at band 14q24	chrb(14)(24)
		Distorted morphology (x4)	pvz
		Tetra-Satellite associations between the 'DDGG' group chromosomes; acrocentric chromosome associations involving chromosomes 14, 15 and 21	
		Tri-Satellite associations between the 'DGG' 'DDD' and `DDG' group chromosomes	
		Di-Satellite associations between the 'DD', DG and GG group chromosomes	
20mM	50 cells	Distorted appearance of chromosomes (8)	pvz
		Polypoidy with multiple gaps in chromosomes	
		Acentric fragment	ace
		Chromosome break at band 1q41	chrb(1)(q41)
		Tri-Satellite associations between the 'DDG' 'DGG' and `GGG' group chromosomes	
		Di-Satellite associations between the 'DD', DG and GG group chromosomes	
40mM	50 cells	Distorted morphology (x5)	pvz
80mM	50 cells	Tri-Satellite associations between the 'DDG' group chromosomes	
		Di-Satellite associations between the 'DD', DG and GG group chromosomes	
		Distorted morphology	pvz

The vast majority of cells analyzed in control (unexposed) lymphocytes demonstrate normal chromosome structure and morphology with only 5 cells (1.25%) observed with aberrant morphology and acrocentric associations in 300 analyzed cells. We clearly observe an increase in abnormal chromosome morphology with an increase in morphologically distorted chromosomes (pvz), premature chromatid and centromere division (pcd) and acrocentric associations with exposure to H_2O_2. In addition, we have observed a wide array of structural chromosome aberrations including chromosome breaks; chromatid breaks; marker chromosomes; ring chromosomes; deletions; chromosome gaps; dicentric chromosomes and chromosome translocations (Figures 13-16). In one instance, a polyploid cell was observed which is a numerical aberration. For the most part at the lower H_2O_2 concentration 5mM the aberrations observed tend to be morphological aberrations (pvz) acrocentric associations and chromatid breaks with a handful of more major abnormalities resulting in small, unidentified marker chromosomes, chromosome gaps and chromosome breaks. As the H_2O_2 concentration increases we

observe the same morphological abnormalities, acrocentric associations and chromatid breaks and a higher frequency of the more severe aberrations previously listed but also including: ring chromosomes; deletions; chromosome gaps; dicentric chromosomes; chromosome translocations and polyploidy. When we analyze the higher H_2O_2 concentrations (40mM and 80mM) we see what can be interpreted as a slightly lower number of abnormal events compared to the other concentrations. This is largely postulated to be due to the high toxicity of H_2O_2 to these cells resulting in a reduction in cell proliferation and potentially an increase in cells with excessive DNA damage, which ultimately leads to cell death (apoptosis).

UV chromosome aberration assay results

The results are presented as above for H_2O_2 with an example of a normal karyotype (Figure 12) and details of the chromosome aberrations identified for each of the tested UV exposures are provided in Table 12.

Figure 12 Normal metaphase and karyotype from control sample subject #38

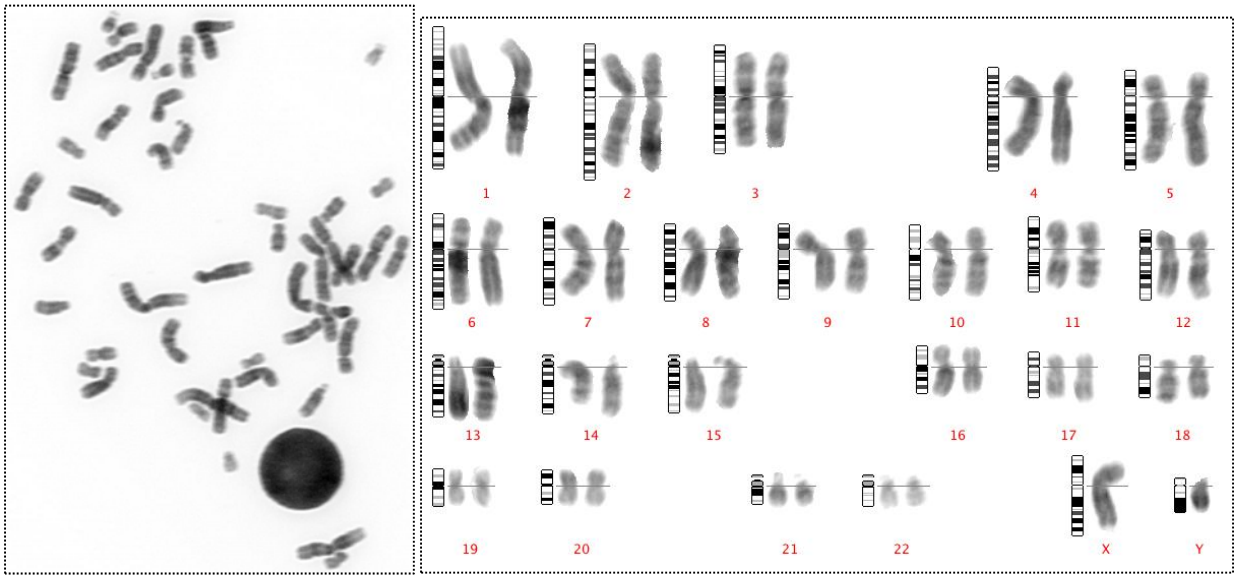

In the few samples completely analyzed for UV exposure no chromosome abnormalities have been observed in the unexposed (control) group. To date, the type of chromosome aberrations observed have also been observed after H_2O_2 treatment but we see a smaller range of abnormalities, which include: distorted morphology (pvz), acrocentric associations, premature chromatid and centromere division (pcd) and chromosome breaks. Our data demonstrate that abnormal morphology and acrocentric associations are observed at an increased frequency in lymphocytes exposed to a longer duration of UV exposure with chromosome breaks observed exposed to a shorter duration of exposure to UV. As with the H_2O_2 treatment this is most likely due to the fact, that, with increasing UV exposure there is a reduction in cell division and an increase in apoptosis.

Table 12 Chromosome aberrations observed after exposure to UV in subject #38

UV treatment	No of cells analyzed	Chromosome aberrations observed (#) indicate multiple cells with aberration	Aberration symbol
+PHA 5min	50 cells	Distorted morphology (x3)	pvz
		Break in chromosome 10 at band 10q25	chrb (10)(q25)
		Break in chromosome 1 at band 1p21	chrb (1)(p21)
		Chromatid break in chromosome 5 at band 5q23	chrb (5)(q23)
		Di-Satellite associations between the 'DD', DG and GG group chromosomes (x8)	
-PHA 5min	50 cells	Chromatid break in chromosome 5 at band 5q23	chrb (5)(q23)
		Distorted morphology (x3)	pvz
		Tri-Satellite associations between the 'DGG' 'DDD' and `DDG' group chromosomes	
		Di-Satellite associations between the 'DD', DG and GG group chromosomes (x8)	
+PHA 10min	50 cells	Distorted appearance of chromosomes (x3)	pvz
		Break in chromosome 6 at band 6p12	chrb (6)(p12)
		Di-Satellite associations between the DG and GG group chromosomes (x2)	
-PHA 10min	50 cells	Distorted morphology (x5)	pvz
		Premature centromere division	pcd
		Tetra-Satellite associations between the 'DDDG' group chromosomes	
		Tri-Satellite associations between the 'DDG' group chromosomes	
		Di-Satellite associations between the `DG' and `GG' group chromosomes	
+PHA 15min	50 cells	Distorted morphology (x2)	pvz
		Tri-Satellite associations between the `DDD' and 'DDG' group chromosomes (x2)	
		Di-Satellite associations between the DD DG and GG group chromosomes (x14)	
-PHA 15min	50 cells	Tetra-Satellite associations between the 'DGGG' group chromosomes	
		Di-Satellite associations between the 'DG' group chromosomes (x2)	
		Distorted morphology (x3)	pvz
+PHA 30min	50 cells	Penta-Satellite associations between the 'DDDGG' group chromosomes	
		Tetra-Satellite associations between the 'DDDG' group chromosomes	
		Tri-Satellite associations between the 'DDG' group chromosomes	
		Di-Satellite associations between the `DD' and `DG' group chromosomes (x9)	
-PHA 30min	50 cells	Distorted morphology (x3)	pvz
		Tri-Satellite associations between the 'DDG' and 'DGG` group chromosomes (x3)	
		Di-Satellite associations between the `DD' `DG' and `GG' group chromosomes (x10)	

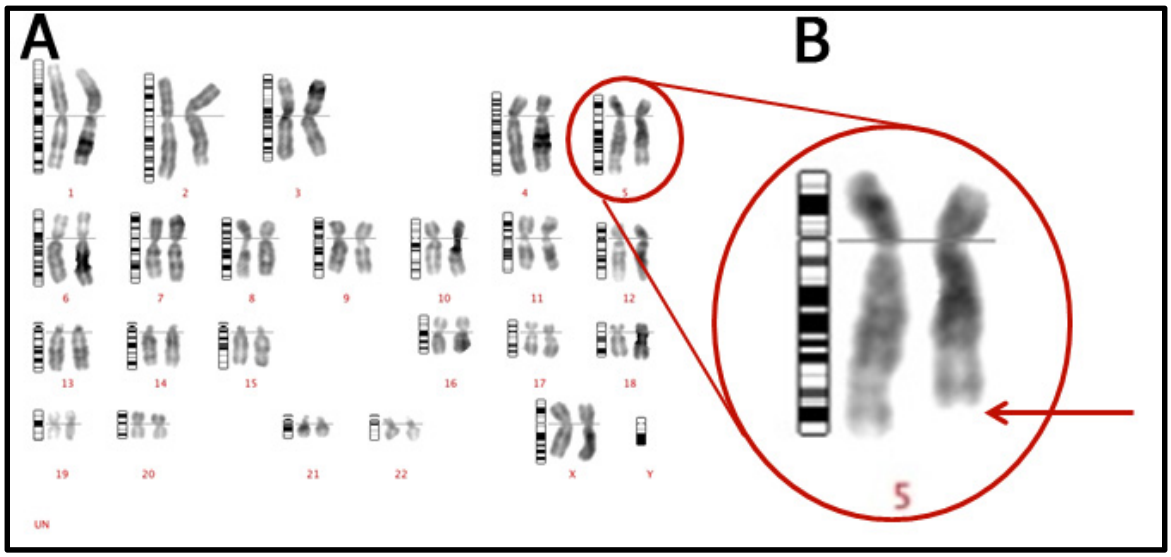

Figure 13: Reverse DAPI banding of a human metaphase spread obtained after incubation for 30 minutes with 10mM H_2O_2, followed by 72 hours of culture, cell fixation with hypotonic treatment and DAPI staining. A) The karyotype obtained shows 46 chromosomes and two X chromosomes and therefore normal in chromosome number. B) However, enlargement of chromosome 5 illustrates a large terminal deletion (arrow) in which a segment of the end of the chromosome has been lost.

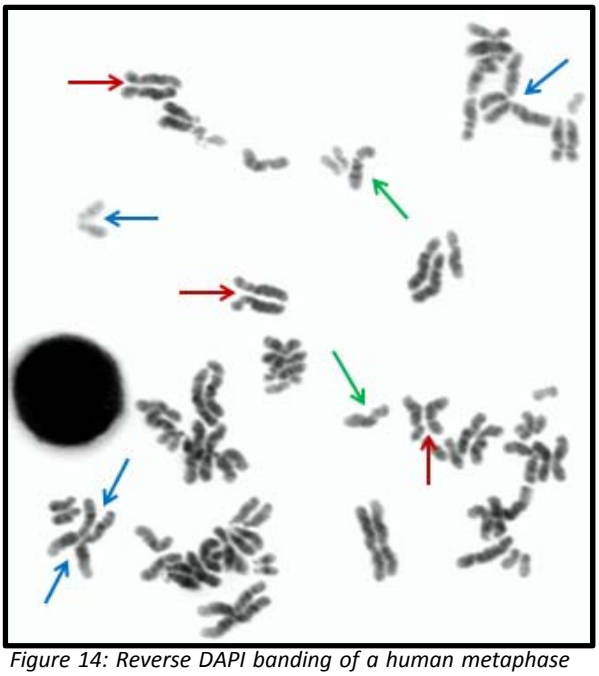

Figure 14: Reverse DAPI banding of a human metaphase spread obtained after exposure to H_2O_2. Metaphase spread demonstrates normal chromosomes (green arrows); premature sister-chromatid separation, where the centromeres are still joined (blue arrows) and premature centromere separation, where there appears to be no connection between centromeres (red arrows).

Figure 15: Observed are multiple chromosomes (some indicated by arrows) demonstrating altered morphology (pvz), (wavy or bent) and indistinct banding pattern making identification difficult. In addition, the location of the centromere (site of the primary constriction) is difficult to identify, appearing as "puffy". These factors in combination make it impossible to identify the vast majority of the chromosomes in this metaphase spread.

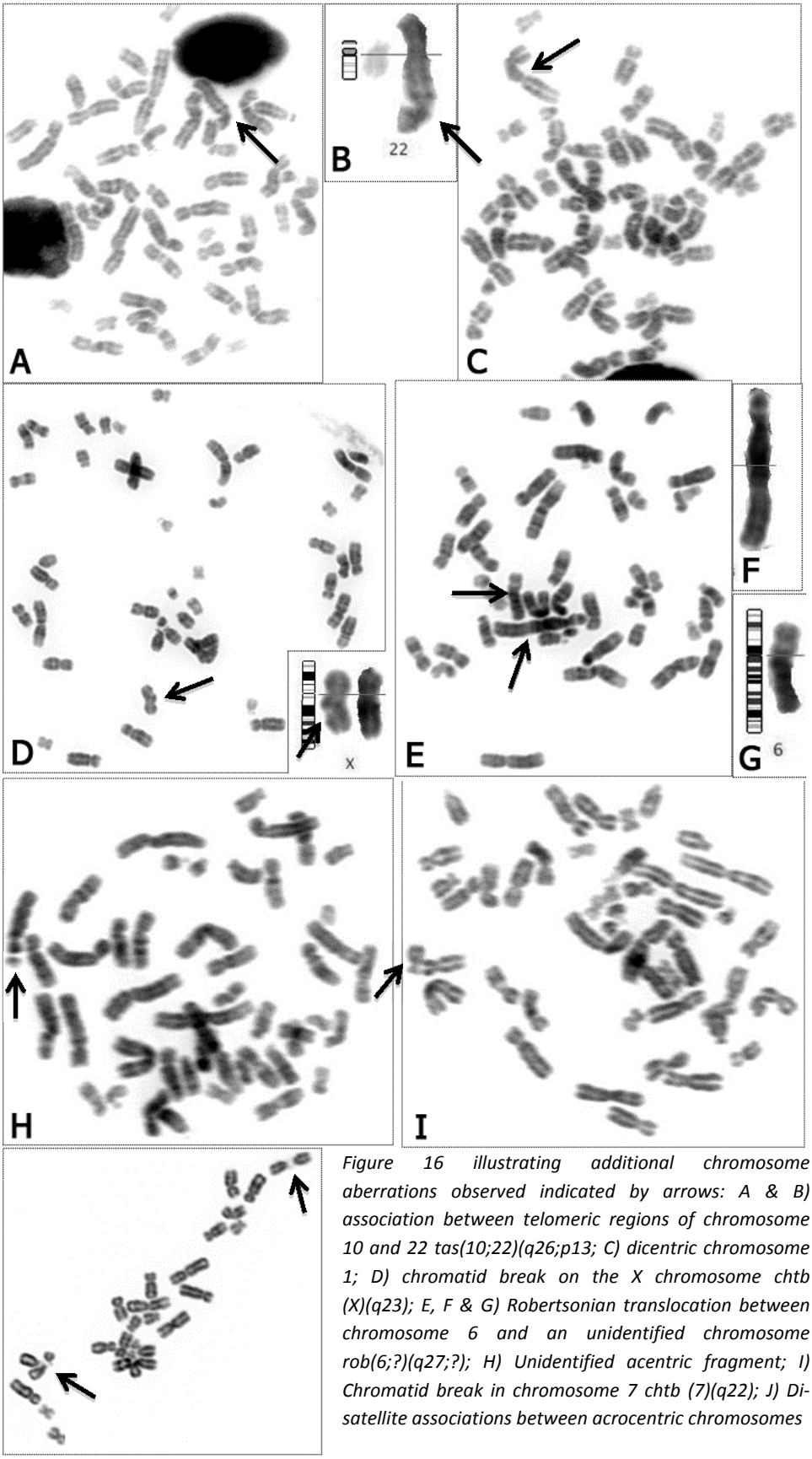

Figure 16 illustrating additional chromosome aberrations observed indicated by arrows: A & B) association between telomeric regions of chromosome 10 and 22 tas(10;22)(q26;p13; C) dicentric chromosome 1; D) chromatid break on the X chromosome chtb (X)(q23); E, F & G) Robertsonian translocation between chromosome 6 and an unidentified chromosome rob(6;?)(q27;?); H) Unidentified acentric fragment; I) Chromatid break in chromosome 7 chtb (7)(q22); J) Di-satellite associations between acrocentric chromosomes

2.1.6. Fluorescence In-Situ Hybridization (FISH)

Fluorescence in-situ hybridization (FISH) allows identification of specific regions of interest in the genome by "fluorescently painting". In brief, the methodology involves DNA probes that can be manufactured in the lab or purchased and correspond to specific regions of the genome (e.g., a single whole chromosome; a small region specific to a certain chromosome such as a gene, centromere or telomere) (Figure 17). These probes can be applied to metaphase chromosomes and interphase nuclei to highlight or "paint" specific regions of interest.

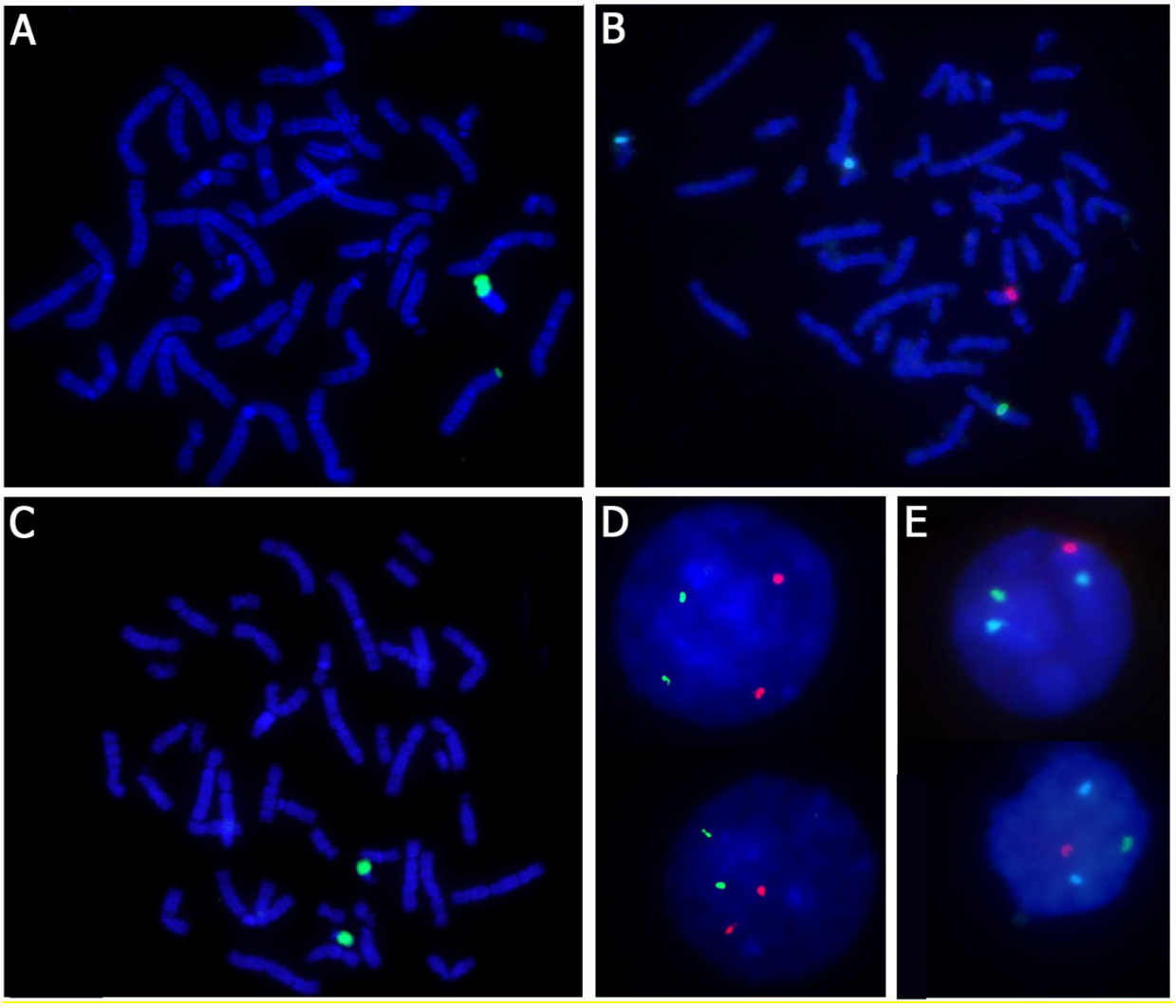

Figure 17: Fluorescent in-situ hybridization images A-E. DNA (interphase nuclei and metaphase chromosomes) is stained with DAPI (blue). A) FISH utilizing whole chromosome paint for chromosome Y (green) on a human metaphase. B) FISH using centromeric probes for chromosome 18 (aqua), chromosome Y (red) and chromosome X (green) on a human metaphase. C) FISH utilizing a whole chromosome paint for chromosome 22 (green) on a human metaphase. D) FISH using locus specific probes for chromosomes 13 (green) and 21 (red) in human lymphocyte nuclei. E) FISH using centromeric probes for chromosome 18 (aqua), chromosome Y (red) and chromosome X (green) in human lymphocyte nuclei.

By denaturing lymphocyte cells or chromosomes target DNA becomes single stranded, potentially enabling a FISH probe to hybridize to its homologous sequence if present in the cell or the chromosome. Hybridization overnight, followed by post-hybridization washes the following day, this allows target DNA to renature with the fluorescent probes incorporated within the target DNA. The target DNA and fluorescent probes are then visualized, captured and analyzed using fluorescent microscopy with associated capture software.

FISH can now be combined with the three DNA damage assays, but prior to this it is essential to establish the experimental parameters for optimal FISH results. We have thus tested a variety of commercially available probes in various target cells (nuclei and chromosomes). These include centromeres, locus specific probes and whole chromosome paints in both interphase nuclei and metaphase chromosomes (Figure 17). We have established the optimum parameters, specifically: pre-treatment of the target material; hybridization temperature, hybridization duration and post-hybridization washes for each of these probe types. FISH will be combined with the various cytogenetic assays dependent on the sensitivity of the biosensors compared to the cytogenetic assays. If deemed necessary and given evidence that one or both biosensors are capable of detecting DNA damage with greater sensitivity than standard cytogenetic assays without the inclusion of FISH. In this case, FISH may be utilized to increase the sensitivity of the cytogenetic assays allowing comparisons to be made with the biosensors.

2.1.7. Micronucleus Assay (MN)

The micronucleus assay is a mutagenicity assay that is capable of detecting agents, which induce the formation of micronuclei in the interphase cytoplasm. These micronuclei may be composed of whole chromosomes or fragments of chromosomes that are unable to segregate to the daughter cells correctly during cell division. The cytokinesis-block assay enables the differentiation between cells that have not undergone cell division (mononucleates) from those that have undergone once cell division (binucleates) or multiple cell divisions (multinucleates) (Figure 18). The cytokinesis-block proliferation index (CBPI) evaluates the effect of cytotoxicity, specifically the impact of the tested substance on cell proliferation. The CBPI is a ratio between the three subpopulations of cells with different numbers of nuclei (mono-, bi- and multi-nucleate cells) and is a measure of the average number of cell cycles that a cell population undergoes.

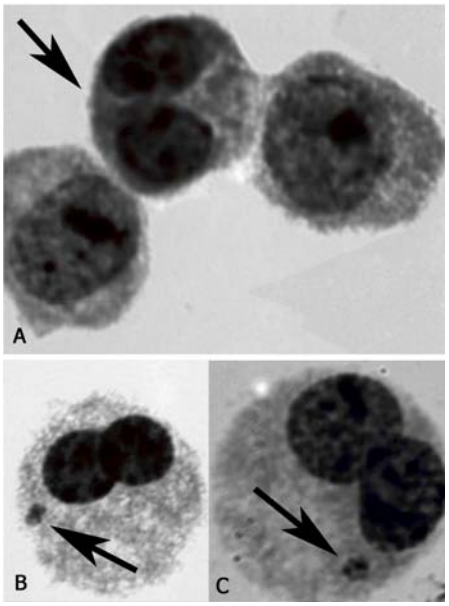

Figure18 Images of lymphocytes cells following the micronucleus assay

A) Image of three cells, two mononucleate cells (cells that have not undergone cell division) and one binucleate (arrowed) (a cell that has undergone cell division. The number of mononucleates, binucleates and multinucleates (not shown) are utilized to calculate the CBPI to provide a measure of cell proliferation

B and C) are examples of cells that have undergone cell division (binucleate) and within which DNA damage has occurred. The result of the DNA damage is a fragment of DNA that has failed to become incorporated within the two new daughter and is extruded from the dividing nuclei as a micronucleus (arrowed)

To date, a total of 8,000 H_2O_2 exposed lymphocytes have been analyzed for the micronucleus assay, lymphocytes were exposed to 0, 0.25, 0.5 and 1mM H_2O_2 for 10 minutes and left to grow in culture for three days to allow micronuclei to form and to investigate the effect of the agent on cell proliferation. The H_2O_2 data is presented in Figures 19 and 20 and clearly demonstrate a reduction in cell proliferation in correlation with increasing exposure to H_2O_2. This can be observed in Figure 19 with increasing numbers of mononucleate cells (cells that have not undergone cell division) and decreasing numbers of bi- and multi-nucleate cells with increasing concentration of H_2O_2. Figure 20 also displays the CBPI which as mentioned previously is a measure of cell proliferation and clearly depicts this trend of a reduction in cell proliferation. In addition, to a reduction in cell division we also observe an increase in the formation of micronuclei (Figure 20). The control (unexposed) lymphocytes were not found to contain any micronuclei, the occurrence of which, was observed at the lowest H_2O_2 concentration the levels of which increased at the concentration of 0.5mM, at the highest concentration we see a small reduction in the number of micronuclei. We believe this to be due to the high concentration that has resulted in very high levels of DNA damage, this high concentration leads to cell death (apoptosis) in those cells that have accumulated significant levels of DNA damage, thus we observe less micronuclei. These results clearly demonstrate that H_2O_2 is capable of inducing micronuclei formation the number of which increases with increasing H_2O_2 concentration, this agent has also been shown to reduce cell proliferation in culture. We have established a good dose response curve with our maximal concentration leading to low levels of apoptosis, higher concentrations tested lead to massive cell death and are hence unanalyzable.

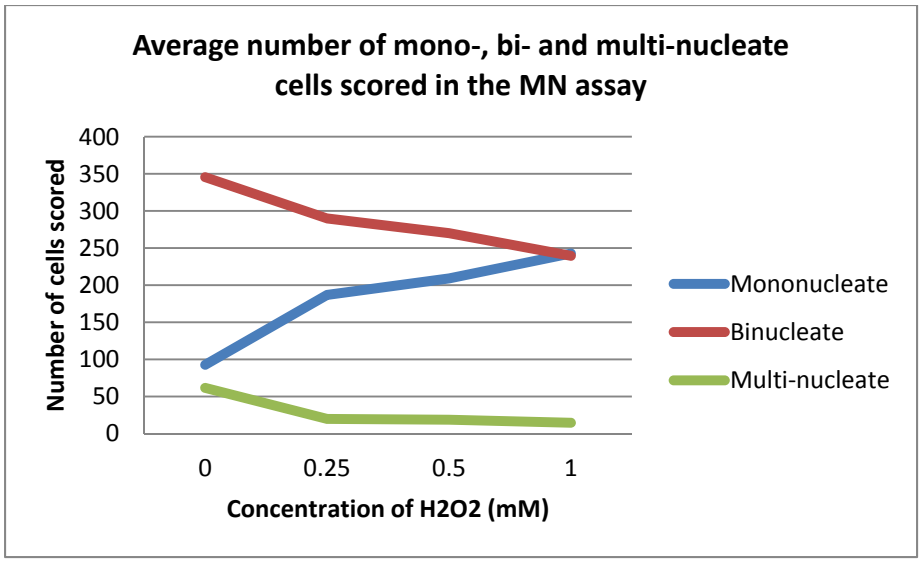

Figure 19 displaying the average number of mononucleate, bi nucleate and multinucleate cells as analyzed with the MN assay in H_2O_2 treated lymphocytes. The graph shows an increase in non-proliferative cells with increasing H_2O_2 treatment and a reduction in proliferative cells (binucleate and multinucleate cells)

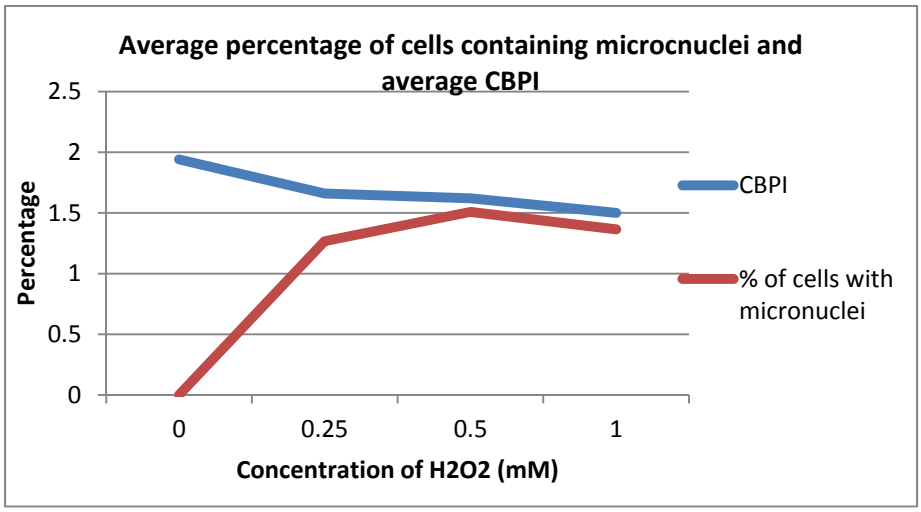

Figure 20 displaying the average percentage of micronuclei observed after H_2O_2 treatment which increases to the highest level at 0.5mM and then drops at 1mM. This reduction in number of micronuclei corresponds well with an increase in non-proliferative cells and a drop in the cytokinesis-block proliferation index (CBPI) also depicted on this graph

Establishing the dose response for the UV exposure has been more problematic we have analyzed over 12,000 cells utilizing different exposures and have failed to get reproducible results as observed in the H_2O_2 MN assay. The data presented in Figures 21 and 22 shows the data collected from lymphocytes exposed to 0, 2, 5 and 7 minutes of UV prior to culture. These data demonstrate that the MN assay in control (unexposed) lymphocytes is working and produces similar results to the H_2O_2 control lymphocytes. However, we see a much larger reduction in cell proliferation (CBPI) even at the lowest exposure (2 minutes) than we observe at the highest H_2O_2 concentration (Figures 22 and 20). In addition, at 5 minutes we observe an increase in mononucleate cells and a decrease in bi- and multi-nucleate cells, at the highest exposure we observe a significant reduction in all cell types due to massive apoptosis. At the highest exposure we are unable to find more than 25 cells, even at the lowest exposure in some patients we observe massive apoptosis which surpasses a 50% reduction in cell

proliferation as outlined in section 2.1.3. We are in the process of reducing the exposure times from 30 seconds to 4 minutes (data not shown), but again we observe massive apoptosis from the 30-second exposure. To date in the 12,000 cells analyzed we have also only observed 3 micronuclei (Figure 22), thus we have concluded that in our hands the mechanism of UV damage does not induce micronuclei and that exposure to isolated lymphocytes to UV followed by a three day culture demonstrates massive apoptosis. We do not observe as high levels of apoptosis in the comet assay even with a 10 minute UV exposure, however, this is likely due to the fact that cells in the comet assay are exposed and processed on the same day and it is a measure of a different DNA damage mechanism. In addition, DNA damage is not accumulated over the culture period and whilst we observe apoptosis in the comet assay the timeframe for which apoptosis can be initiated is more limited than in the MN assay.

Figure 21 displaying the average number of mononucleate, bi nucleate and multinucleate cells as analyzed with the MN assay in UV exposed lymphocytes. The graph shows an increase in non-proliferative cells with increasing UV treatment and a reduction in proliferative cells (binucleate and multinucleate cells)

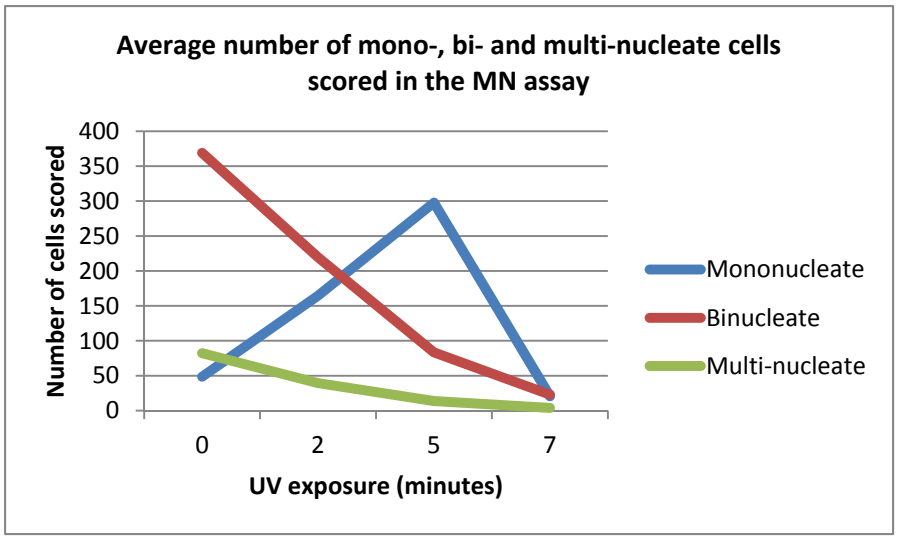

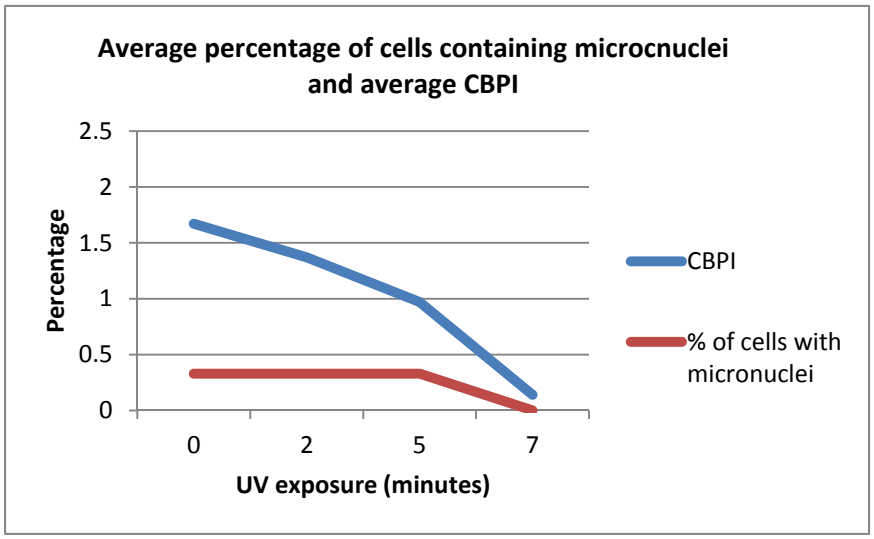

Figure 22 displaying the average percentage of micronuclei observed after UV exposure. A very low percentage of MN are observed at all concentrations with the exception of 7 minutes. We observe an increase in non-proliferative cells and a significant drop in the cytokinesis-block proliferation index (CBPI) also depicted on this graph

2.1.8. Comet Assay

Isolated lymphocytes have been cultured in the presence of H_2O_2 or exposed to UV at different concentrations or duration of exposure, respectively, for both assays control experiments were also processed in which isolated lymphocytes were not exposed to either H_2O_2 or UV. The comet assay measures the amount of single and double-stranded DNA damage present (as described in section 1.1.), in this case after exposure to genotoxic agents. After performing the comet assay intact DNA (no- very low levels of DNA damage) the DNA remains associated within the cell nucleus (comet head), with increasing levels of DNA damage the DNA migrates out of the cell nucleus producing the comet tail (Figure 23). Initially we were working with the company that provides our microscopy capture software to develop our own in house software to perform the quantitative analysis, however, the software developed was not able to produce reproducible results for control/low levels of DNA damage. Therefore we purchased commercially available software from Perceptive instruments. The software quantitatively measures the amount of fluorescence (which correlates to the amount of DNA present) in the comet head (cell nucleus) and the comet tail (Figure 24). For the comet assay the isolated lymphocytes are exposed to concentrations of H_2O_2 of 0.25mM, 0.5mM and 1.0mM for 10 minutes and exposed to UV for 2, 5 and 10 minutes prior to being processed for the comet assay. To date, we have processed and completed the comet assay analysis of 14 subjects analyzing a total of 2,800 cells, the results for the eight samples exposed to H_2O_2 and six samples exposed to UV are presented in Table 13, Figure 24 and Table 14 Figure 25 respectively.

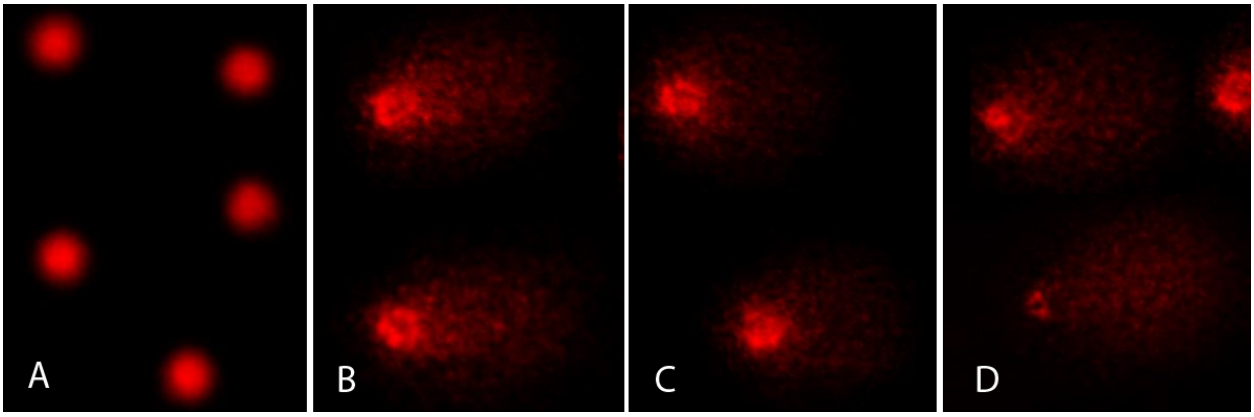

Figure 23: Lymphocyte cells stained with propidium iodide after comet assay processing. A) control unexposed lymphocytes, cells which retain the normal cell nuclei morphology with little diffusion of DNA outside the nucleus (comet head). Lymphocytes in panels B, C and D have been exposed to increasing concentrations of H_2O_2 (0.25mM, 0.5mM and 1.0mM respectively). These lymphocytes demonstrate altered nuclear morphology with increasing diffusion of DNA out of the nucleus (comet tail).

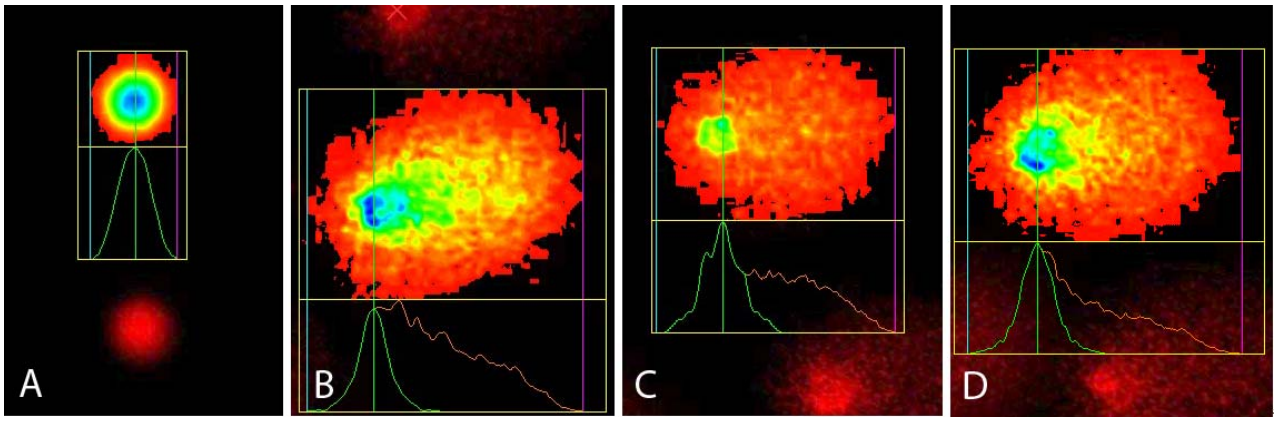

Figure 24: Lymphocyte cells stained with propidium iodide analyzed by Comet Perceptives software. The software utilizes the fluorescence intensity to measure the amount of DNA present in the cell nucleus (head) and the amount that is present in the comet tail. In this series of images A) represents control unexposed lymphocytes, cells which retain the normal cell nuclei morphology with little diffusion of DNA outside the nucleus. Lymphocytes in panels B, C and D have been exposed to increasing concentrations of H_2O_2 (0.25mM, 0.5mM and 1.0mM respectively). These lymphocytes demonstrate altered nuclear morphology with increasing diffusion of DNA out of the nucleus (comet head) with less measurable fluorescence intensity in the nucleus and increasing concentration of DNA (measured by fluorescence intensity) in the comet tail.

Table 13 H_2O_2 comet assay results in eight subjects. Table provides the average percentage of DNA within the comet head and the comet tail for the different H_2O_2 concentrations

	Control		**0.25mM**		**0.5mM**		**1.0mM**	
Subject #	% of DNA in Head	% of DNA in Tail	% of DNA in Head	% of DNA in Tail	% of DNA in Head	% of DNA in Tail	% of DNA in Head	% of DNA in Tail
30	97.73	2.27	77.53	22.47	53.71	46.29	31.51	68.49
32	95.36	4.64	31.70	68.30	22.55	77.45	16.67	83.33
33	98.58	1.42	46.07	53.93	34.74	65.26	16.42	83.58
34	97.68	2.32	54.65	45.35	51.92	48.08	37.31	62.69
40	98.20	1.80	61.69	38.31	37.25	62.75	18.81	81.19
44	99.94	0.06	78.62	21.38	64.50	35.50	42.78	57.22
48	99.98	0.02	88.09	11.91	57.00	43.00	28.98	71.02
50	97.85	2.15	56.16	43.84	34.04	65.96	22.36	77.64
Average	**98.17**	**1.83**	**61.81**	**38.19**	**44.46**	**55.54**	**26.85**	**73.15**

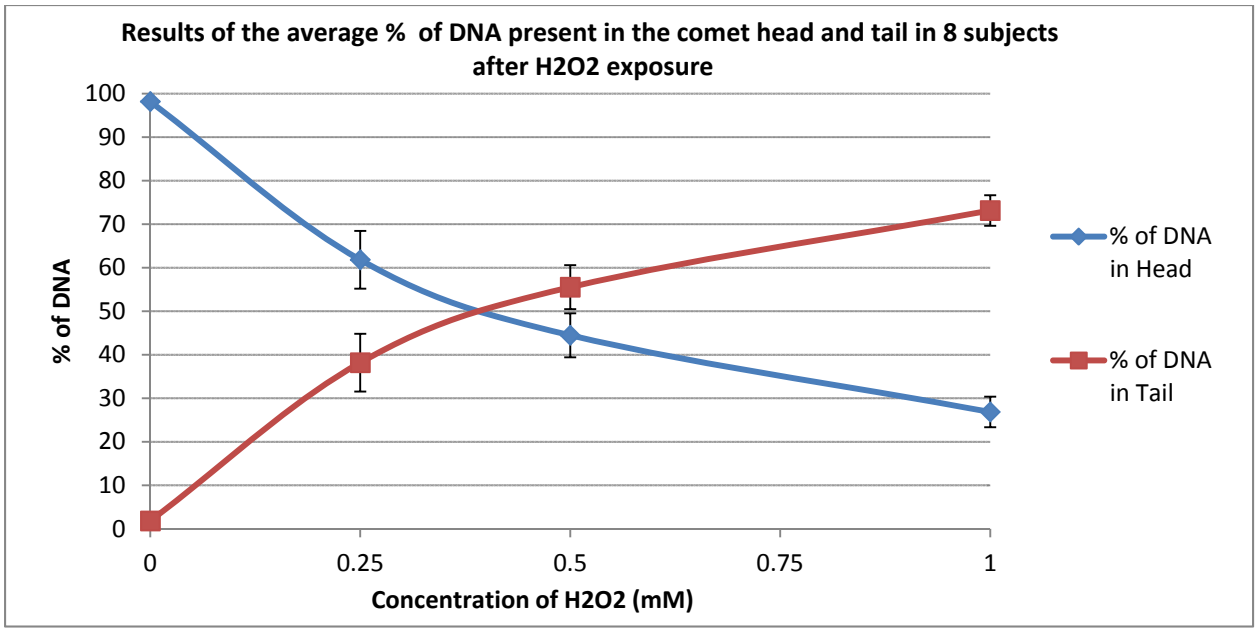

Figure 24 results from table 13 displayed graphically showing the average percentage of DNA within the comet head and the comet tail for the different H_2O_2 concentrations within the eight subjects

Table 14 H_2O_2 comet assay results in six subjects. Table provides the average percentage of DNA within the comet head and the comet tail for the different durations of UV exposure

	Control		**2 minutes**		**5 minutes**		**10 minutes**	
Subject #	% of DNA in Head	% of DNA in Tail	% of DNA in Head	% of DNA in Tail	% of DNA in Head	% of DNA in Tail	% of DNA in Head	% of DNA in Tail
35	94.32	5.68	46.56	53.44	16.10	83.90	13.45	86.55
36	99.40	0.60	45.21	54.79	23.88	76.12	16.53	83.47
38	99.03	0.97	74.10	25.90	31.38	68.62	26.22	73.78
42	98.62	1.38	80.73	19.27	69.41	30.59	42.53	57.47
45	99.63	0.37	78.48	21.52	18.57	81.43	19.63	80.37
50	96.11	3.89	64.20	35.80	25.46	74.54	37.37	62.63
Average	**97.85**	**2.15**	**64.88**	**35.12**	**30.80**	**69.20**	**25.96**	**74.04**

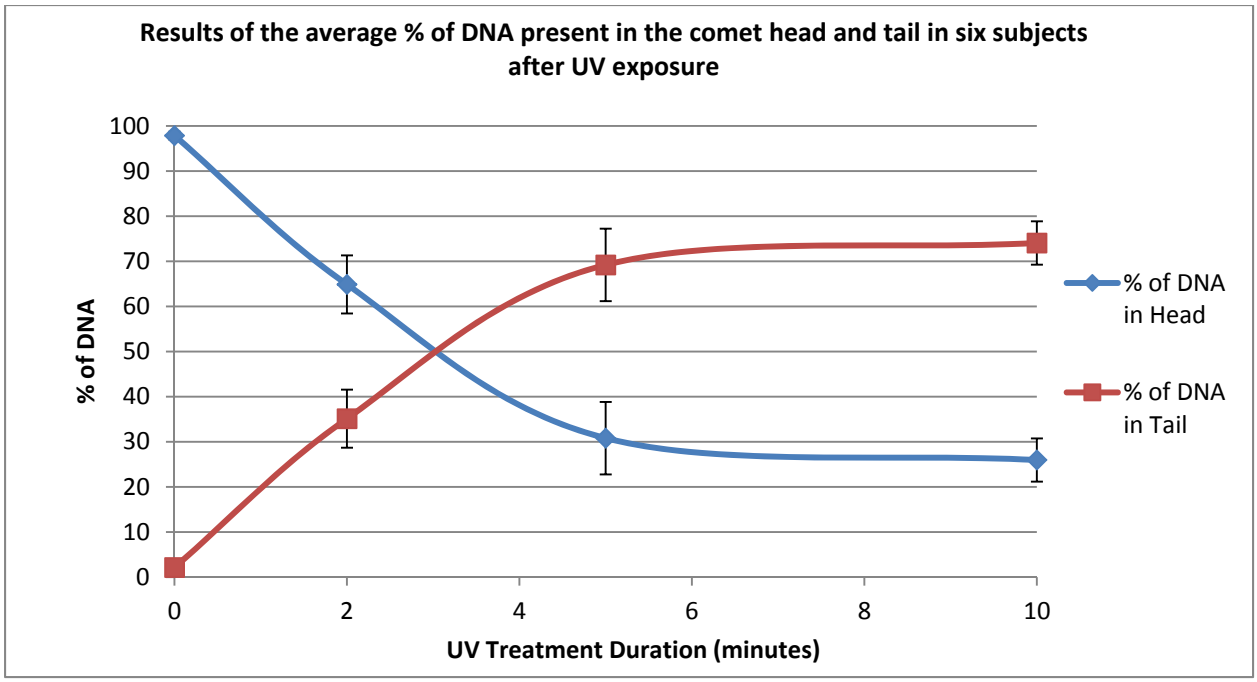

Figure 25 results from table 14 displayed graphically showing the average percentage of DNA within the comet head and the comet tail for the different UV exposures within the six subjects

The data from the comet assay clearly demonstrate that we are capable of inducing single- and double-stranded DNA damage with both our genotoxic agents (H_2O_2 and UV) at the concentrations and exposures chosen. We observe a good dose response for both agents with increasing DNA damage seen with increasing genotoxic concentration and exposure (Tables 13-14 and Figures 24-25). The control samples demonstrate very low levels of DNA damage for both H_2O_2 and UV with approximately 98% of DNA being retained in the cell nucleus in the 700 cells analyzed for the unexposed samples. We observe a well-defined increase in single- and double-stranded DNA breaks even at the lowest concentration/exposure of the genotoxic agents with approximately 62-64% of DNA being retained in the cell nucleus. Thus, at these concentrations we observe that 35-39% of the DNA of the cell is associated with DNA damage. As the concentration or exposure of the genotoxic agents increases further DNA damage is induced (56-69% with 44% and 31% retained in the cell nucleus respectively). Our maximal level of DNA damage (73-74% with 26-27% retained in the cell nucleus) is observed with our highest H_2O_2 concentration 1.0mM and 10 minute UV exposure. The comet assay in our hands has provided an excellent dose response relationship in which we observe the DNA damage induced correlated with increasing concentrations or exposure of the genotoxic agent. We observe no significant difference in the amount of single- or double-stranded DNA breaks induced by either of the genotoxic agents at the concentrations or exposures chosen. From this data we can conclude that the 14 tested samples had very low baseline levels of DNA damage and that both genotoxic agents chosen are capable of inducing low to high levels of single- and double-stranded DNA breaks depending on the concentration and exposure duration of the agent in question.

2.2. EIST Based Biomarker Sensor For Oxidative DNA Damage Assessment

OVERALL OBJECTIVES: The overall goal of this stage of the project (2010-2012) is to develop a paper-based biosensor which integrates the immunochromatography method and electrochemical method for qualitative and quantitative detection of the DNA oxidative damage biomarker-8 hydroxy-2-deoxy-guanosine (8-OHdG). Human urine samples will be used to assess toxic exposure assessment. Based on previous year's accomplishments, the research focuses of 2011-2012 are mainly on: 1. Quantitative analysis of the biomarker using ImageJ software; 2. DNA Damage Assessment of UV and H_2O_2 on Lymphocytes cells by testing 8-OHdG level in cell culture medium; 3. 8-OHdG detection by CNT paper-based electrochemical method, the detail report as shown below.

2.2.1. Quantitative analysis of the biomarker using ImageJ software

Quantitative analysis of the standard 8-OHdG solution

A series of 8-OHdG standard solutions with concentrations of 0, 0.1, 1, 10, 50, 100, 500, 1000, 10000, and 100000 ng mL^{-1} in 1X PBS buffer were prepared and applied to the strips. After 15 min, photographs were taken by using a digital camera, and then specific software was used for quantitative analysis (ImageJ) (Liu et al., 2011)

Figure 26 shows the typical responses of the lateral flow immunoassay (LFIA) to 8-OHdG with increasing concentrations from 0 to 100000 ng mL^{-1} dissolved in 1X PBS. The color intensity of the test line decreased when the sample concentration increased in general, which was consistent with the theory of detection of competitive format. The visual detection limit is defined herein as the minimum target analyte concentration required by the T-line for showing no obvious staining effect. Following this definition, the visual detection limit achieved by the standard sample is above 1000 ng mL^{-1}. The visual detection range is from 0 to 10000 ng mL^{-1}.

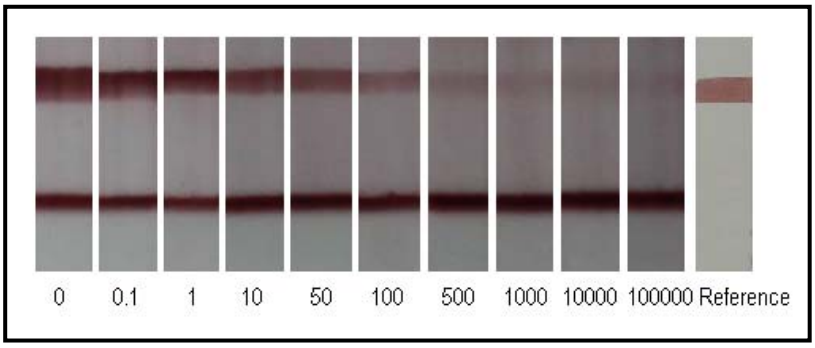

Figure 26. *Photographs of test strips of LFIA based on standard samples (8-OHdG was dissolved in 1X PBS). Top line: Test-line; Bottom line: Control-line. The concentration unit for those shown on the bottom is ng/mL.*

In order to quantitatively extract the detection limit and detection range of this LFIA method, the test strips were further subjected to optical density analysis. The signals from both the T-line averaged from three parallel runs, and one from red color tape (reference) were digitized to optical density using ImageJ software and expressed by the integral area of the cross-section of the T-line (areaT) and reference-line (areaR) within a fixed peak width. In order to eliminate the influence of artificial effects, a relative optical density (ROD) defined as areaT/areaR was used in the signal analysis. The optical density

profiles of both the T-line and C-line (control) recorded under different analyte concentrations are shown in Figure 27 (a) with the optical densities of the T-line and C-line being normalized with respect to that of baseline. The optical intensity of the T-line obviously increased with decreasing analyte concentration. The discrimination of intensities is more intuitive compared to the photograph taken by the camera.

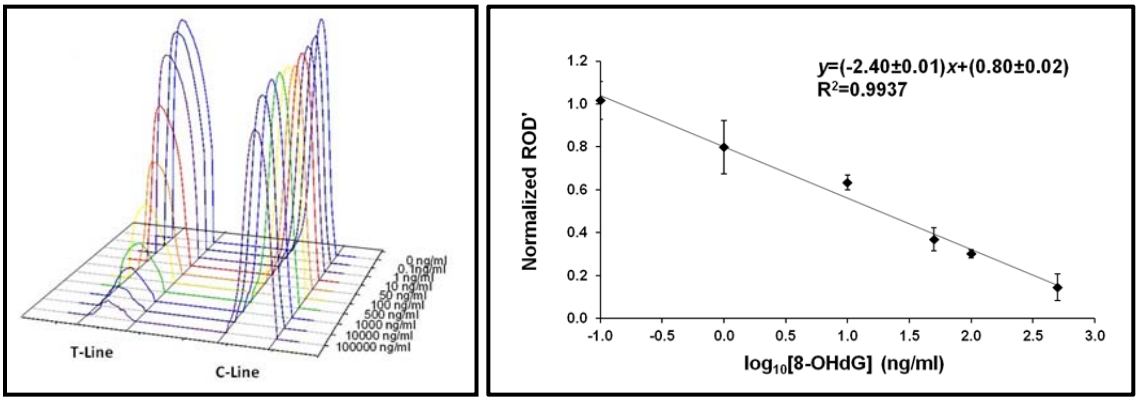

Figure 27. (a) Optical density profiles of the T-line and C-line recorded by using software ImageJ and Sigmaplot after running a series of standard solutions with different 8-OHdG concentrations dissolved in 1X PBS; (b) Dose-response curves for 8-OHdG based on optical density analysis using standard samples. Values are mean SD from three independent experiments.

Considering the actual situation, the meaningful research range for 8-OHdG is from 0 to 500 ng mL^{-1}. To extract the detection limit of the current LFIAs, the ROD' defined as ROD/ABD (average blank density) of the T-line is plotted against the concentration of 8-OHdG in the logarithm scale as shown in Figure 27 (b). Linear fitting of the dose-response curves suggests that the linear response range of the standard sample is from 0.1 to 500 ng mL^{-1} with a correlation coefficient of 0.9937. With the definition of the detection limit as the minimum concentration of analyte required for inducing a 10% ROD' decrease, it was determined as 0.9 ng mL^{-1} for standard sample.

Quantitative analysis of the 8-OHdG spiked urine samples

We collected a handful of urine samples from non-smoking, healthy students within department following the IRB protocol. The collected urine samples were centrifuged and the supernatants were filtered through Whatman No.1 filters， and then stored at -20 °C until use. 8-OHdG spiked original urine and diluted (10X) urine with different concentration (Blank, 0.1, 1, 10, 50, 100, 500, 1000, 10000 and 100000 ng/ml) were prepared and applied to the strips. After 10-15 min, photographs were taken using a digital camera [Figure 28 (a) and (b)], subsequently ImageJ software was used for quantitative analysis as illustrated above.

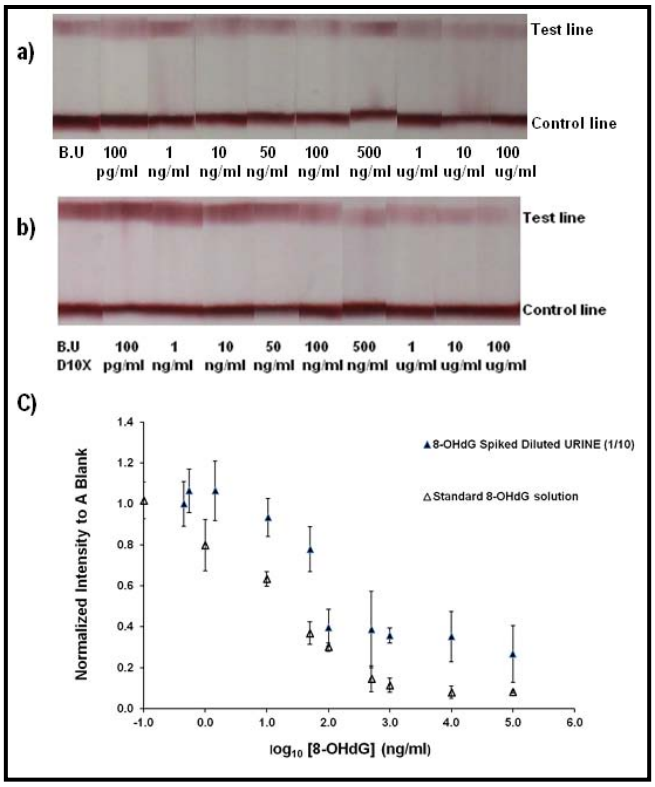

Figure 28. a) Colors indicated on test line and control line with different concentrations of 8-OHdG spiked in original urine; b) Colors indicated on test line and control line with different concentrations of 8-OHdG spiked in diluted (10x) urine; c) Comparison of the data from standard 8-OHdG solution with that from diluted (10x) urine samples.

Before processing data directly from the urine sample, the original 8-OHdG concentration of the urine sample was calculated from the calibration curve obtained from the standard solutions. The concentrations of 8-OHdG in original urine and diluted (10X) urine were 42.94 ng/ml and 0.45 ng/ml, respectively. From the disproportionate data, we know that the situation is more complex in the urine samples compared with the standard solution.

We calculated the total 8-OHdG concentration of urine samples and utilized the logarithm of concentration as the x-axis, and the normalized intensity to blank as the y-axis. Comparing the new graphs obtained from urine samples with the standard curve [Figure 28 (c)], we identified that the error of original urine is too big for calibration. But the result of diluted urine was possible, the reason for this is obvious that there are many molecules that exist in the original urine and the concentration can't be ignored which could affect the reliability of testing. After dilution, the effect is reduced and the result was found to be more reliable. Therefore we conclude that pre-treatment (i.e filtration and dilution) is required for processing of urine samples. But all the results obtained either from the original urine sample or from the diluted urine sample are possible, and have demonstrated the same trend as observed in the standard curve. **Conclusion: The strip can be used for the quantitative analysis of colorimetric testing of both standard 8-OHdG solution and spiked diluted urine samples.**

2.2.2. DNA Damage Assessment of UV and H_2O_2 on Lymphocytes cells by testing 8-OHdG level in cell culture medium

After confirming the feasibility of this strip for 8-OHdG testing, it then can be used for the toxicity assessment in cells. Here we use 8-OHdG as a biomarker to demonstrate the toxic effects caused by exposure the Lymphocytes cells in culture to UV and H_2O_2.

Established a calibration testing curve of 8-OHdG in RPMI cell growth medium

A series of 8-OHdG solutions with concentrations of 0, 1, 10, 20, 40, 80, 100, 150, 200 and 400 ng mL^{-1} in cell-culture medium (RPMI) were prepared and applied to the strips. The cell-culture media (supernatants) after UV and H_2O_2 exposure were also applied to the strips. After 15 min, photographs were taken utilizing photo scanner and subsequently ImageJ software to perform the quantitative analysis as illustrated above. Figure 29 (a) demonstrates that the optical intensity decreased when the concentration of 8-OHdG increased in the cell-culture medium (RPMI), consistent with the mechanism of the competitive format and can, therefore, be used as a calibration standard.

Test 8-OHdG in cell-culture medium after lymphocyte cell exposure to UV

Test 8-OHdG in cell growth medium (RPMI) after exposure of cells (Lymphocytes) to UV (two methods: I. Addition, of phytohemagglutin and exposure with UV; II. exposure with UV followed by addition of phytohemagglutin). Cell-cultures were exposed to different durations of UV exposure 0, 15, 30, 45, and 60 min, and cultured for 72 hours for the chromosome aberration assay (Dr. Tempest's lab). At the end of culture aliquots of the culture media supernatant were removed and stored at -80°C and subsequently tested. From the figure 29 (b), we can see that cells treated with UV (10-20 ng/ml) have higher levels of DNA damage biomarker in the growth medium compared with the control (0-10 ng/ml); method II (15-20 ng/ml) lead to higher DNA damage compare with method I (10-15 ng/ml); Treated cells with UV for 45 min lead to the highest DNA damage (more than 20 ng/ml).

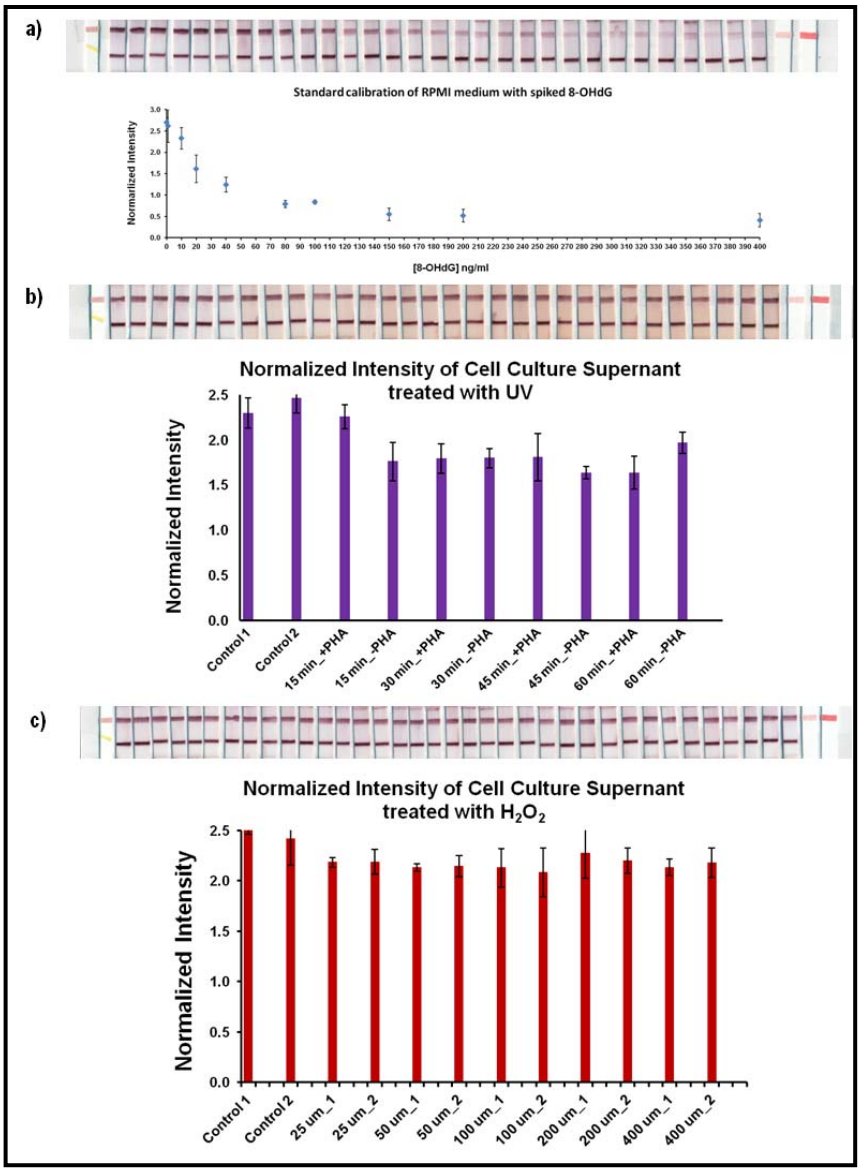

***Figure 29**: a) Standard Calibration for 8-OHdG in RPMI Medium; b) Treat cells by UV; c) Treat cells by H_2O_2.*

Test 8-OHdG in cell culture medium after expose cells to H_2O_2

Testing of 8-OHdG in cell growth medium (RPMI) after cells were exposed (lymphocytes) to hydrogen peroxide (H_2O_2) with different concentrations: 0, 25, 50, 100, 200, and 400 um for 30 min for the CA assay followed by culture for 72 hours (Dr. Tempest's lab). As with the UV experiments aliquots of the culture media were tested at the end of the culture period. From figure 29 (c), we observe that cells treated with H_2O_2 (10-15 ng/ml) have higher DNA damage biomarker in growth medium compared with the control (0-5 ng/ml); Treated cells with 100 um H_2O_2 lead to the highest DNA damage (about 15 ng/ml). **Conclusion: This strip can provide a useful method for DNA oxidative damage assessment in cells with high sensitivity, simplicity and speed of performance.**

2.2.3. 8-OHdG detection by CNT paper-based electrochemical method

The strip designed as detailed above can provide a simple and fast test for DNA oxidative damage. However, one limitation of chromatography is the sensitivity and accuracy. We require a more quantitative method; therefore, we integrated a carbon nanotube (CNT) paper-based electrode with the strip [Figure 30 (a)]. 8-OHdG has redox properties and thus, can be detected by an electrochemical method. The combination of the electrochemical detection and the lateral flow strip based chromatography will provide simple, rapid, and sensitive biosensors for assessment of unspecified DNA and cellular damage.

Characterization of CNT paper

Prior, to using the CNT paper to manufacture the strip, we characterized the CNT paper by using SEM [Figure 30 (b)] to demonstrate the surface structure of CNT.

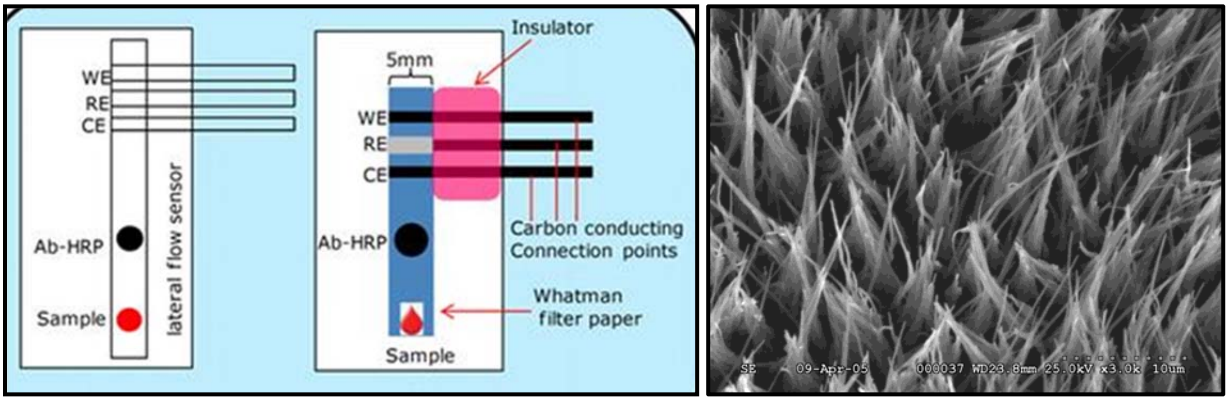

***Figure 30**. (a) Concept of integrating the CNT paper into the traditional lateral flow immunostrip; (b) SEM characterization of CNT paper*

Design for multiple detection of 8-OHdG by CNT paper based electrochemical method

Carbon nanotube (CNT) paper (4 mm in width) was put on a plastic backed plate at the position where the control line is located, and this extra part was laminated with a wire (silver plated copper) which will be connect to a portable potential stat as the working electrode. Silver/Silver Chloride Reference

Electrode (4 mm in width) was placed next to the CNT paper with a 2 mm distance on the side farthest from the sample pad as the reference electrode. Furthermore, nitrocellulose membrane (labeled with test and control lines) was placed on the top to cover the two electrodes. Finally, all other parts, including the sample application pad, conjugate pad and absorption pad were placed at the correct position on the same plastic backing plate [Figure 31 (a)].

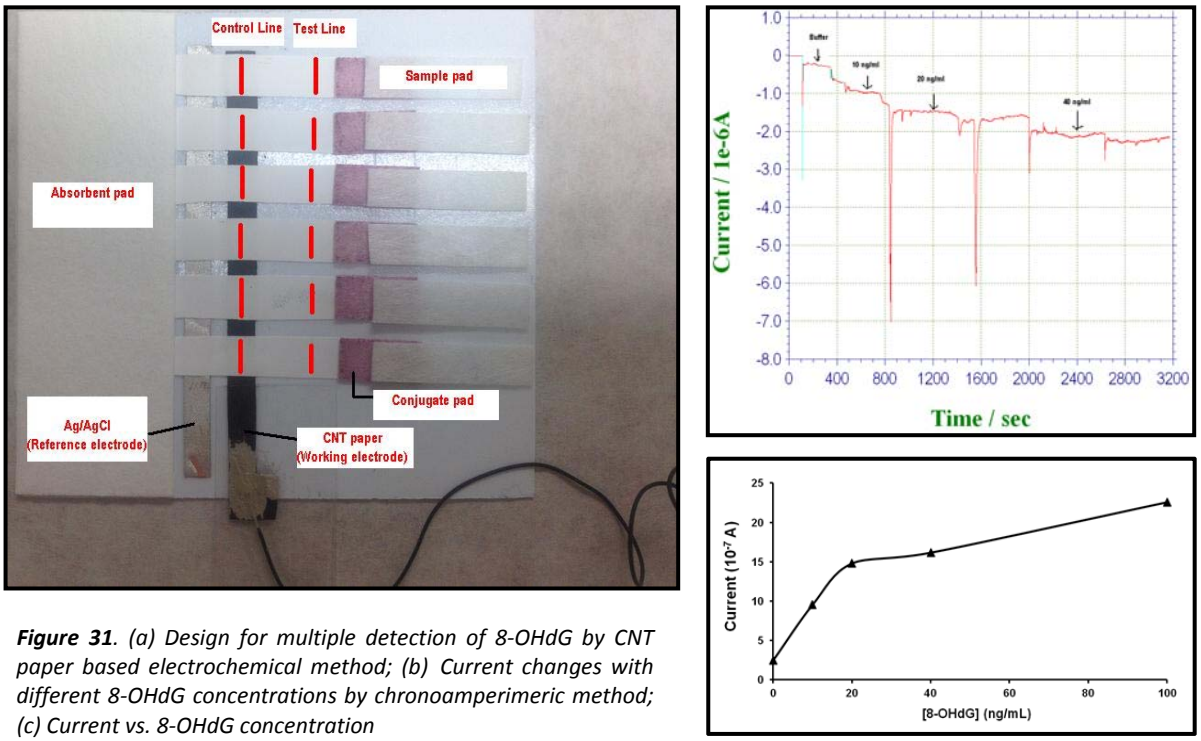

***Figure 31**. (a) Design for multiple detection of 8-OHdG by CNT paper based electrochemical method; (b) Current changes with different 8-OHdG concentrations by chronoamperimeric method; (c) Current vs. 8-OHdG concentration*

Test the feasibility of multiple detection of 8-OHdG by CNT paper based electrochemical method

100 uL of a sample solution (sample 1) containing a desired concentration of 8-OHdG is applied to one sample application zone. Concurrently, chronoamperimeric measurements were performed through software. After waiting for a desired time (for example, 5 min), another 100 uL sample 2 is added to the second sample pad. The above procedure was repeated until six sample pads were utilized, after which, an additional 5-10 min was waited prior to stopping the measurements. Thus, providing a series of current data (I) with various 8-OHdG concentrations [Figure 31 (b)].

Figure 31 (c) shows the preliminary data of the current trend with increased 8-OHdG concentrations. Generally, the absolute current value increased with increasing concentration, which is consistent with the theory. And the detection limit can reach as low as 1 ng/ml. More sensitive results can be obtained by reducing the sensing surface of working electrode at the next stage.

Conclusion: CNT electrode integrated EIST can be used for 8-OHdG detection with high sensitivity. The multiple detection design can provide a high throughput analytical method which is capable of mass screening in toxicological investigations.

2.3. SERS Based Gold Nanoparticle Whole-Cell Biosensor

OVERALL OBJECTIVES: The overall goal of the project is to develop a whole cell SERS sensor based on gold or silver nanoparticle to detect and quantify the expressed stress proteins, Hsp*70, RAD54 and Caspase-3 in yeast cells for the toxic exposure assessment*

2.3.1. Synthesis of two types of SERS substrates; Gold and Silver Nanoparticles

Conventional Gold Nanoparticles (AuNPs) and Silver Nanoparticles (AgNPs) were synthesized using single step citrate reduction method (Lee et al., 1982). Briefly; sodium citrate was added to the salts of Au and Ag under boiling conditions until a wine red Au or yellow greenish Ag color appeared to indicate the synthesis of NPs. The shape and size of the NPs were characterized using microscopy (TEM) and spectroscopy (UV-Vis and DLS). Citrate reduced AgNPs are abbreviated as Ag_{cit} in the following section.

Au and AgNPs synthesized using conventional single step citrate reduction method had comparable shape (spherical) and size (~ 50 nm) (Figure 32)

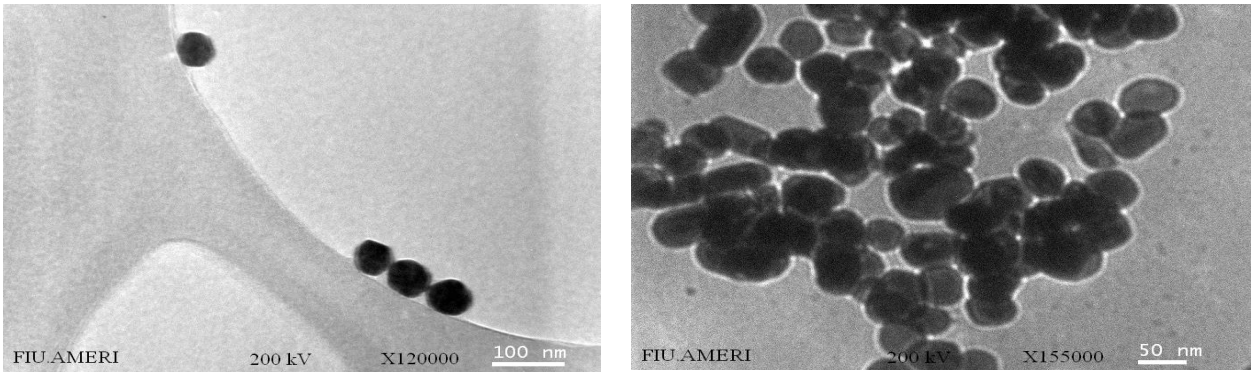

Figure 32: TEM characterization left) AuNPs right) AgNPs

2.3.2. Testing of SERS potential of Au and Ag NPs

Gold and silver NPs synthesized above were tested for their SERS potential under similar conditions (acquisition time of spectra, laser exposure at sample, ratio of analyte to SERS substrate) by adsorbing analytes in free form to the two SERS substrates, Au and Ag NPs, without any aggregating agent. The analytes adsorbed were chemical (MMT linker) and biological (Ab and peptide) in nature and relevant to our study (Figure 33).

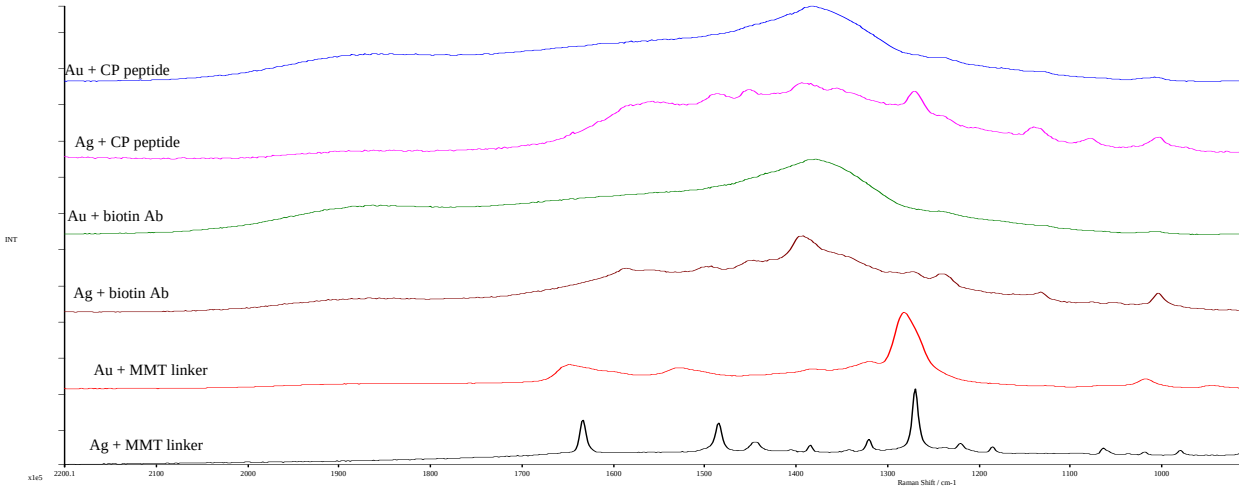

Figure 33: SERS spectra of 3 analytes acquired in presence of two SERS substrates (total 3x2= 6 spectra). Ab: Antibody (biotin), MMT: Mercapto-methyl thiazole acetic acid, CP: Cell Permeability Peptide (TATHA2)

AgNPs produced a larger signal enhancement than AuNPs and convinced us to use push it further as substrate for developing SERS sensor to detect stress markers intracellular and extracellular (in lysate).

2.3.3. Binding of Antigen with Antibody Functionalized and Linker Attached Silver Nanoparticle Surface Assembly of Linker (Mercapto-methyl thiazole acetic acid) onto Silver Nanoparticles

Heterobifunctional cross linker mercapto-methyl thiazole acetic acid (MMT) possessing sulfhydryl and carboxyl groups at its two ends was allowed to self assemble onto silver colloids for extended incubation times (several days). These self-assembled colloids were further centrifuged, washed and characterized using UV-Visible spectroscopy and Raman Spectroscopy. As observed in Figure 34, a red shift of 10 nm in the localized Surface Plasmon Resonance (LSPR) peak of silver colloids along with surface plasmon dampening was observed after linker self- assembly with silver colloids.

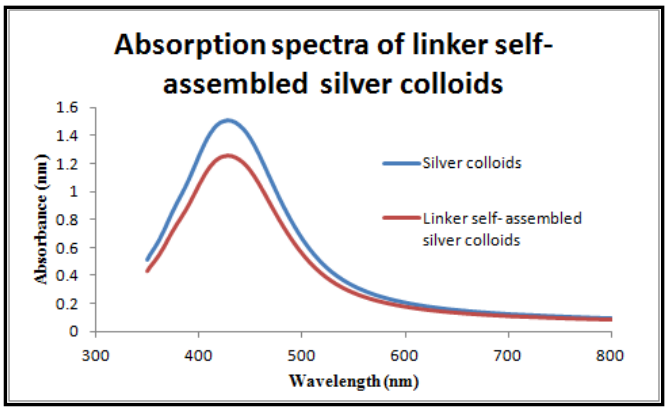

Figure 34: Absorbance Spectrum of Silver Colloids Before and After Self-Assembly of Linker

The linker is characterized through Surface enhanced Raman spectroscopy (Figure 35). Two characteristic peaks around 1300 cm-1 depict the linker.

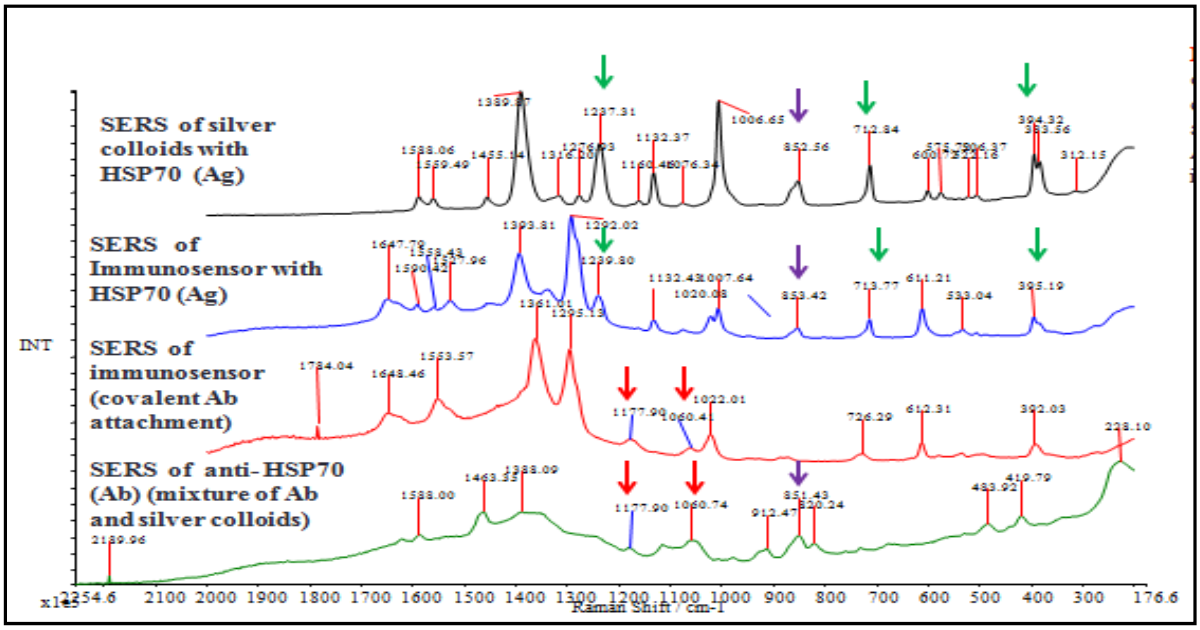

Figure 35. Comparison of SERS spectra of anti-Hsp70 covalently conjugated to silver colloids, anti- Hsp70 physisorbed onto silver colloids, Hsp70 physisorbed with silver colloids and interaction of immunosensor with antigen (Hsp70). Red arrows: denote presence of peaks associated with antibody in the immunosensor; Green arrows: denote presence of antigen peaks in immunosensor interacting with antigen and Purple arrows: Denote antibody and/ or antigen peaks in immunosensor interaction with antigen.

Antibody Conjugation onto Linker Self-Assembled Silver Colloids:

Linker assembled silver colloids were reacted with 1-Ethyl-3-(3-dimethylaminopropyl) carbodiimide (EDC) and N- Hydroxysuccinimide (NHS) to activate the carboxyl groups. These activated silver colloids were then incubated with anti-Hsp70 to yield antibody- conjugated silver colloids. These antibody conjugated silver colloids were characterized by UV-Visible spectroscopy and Raman Spectroscopy. Similar conjugation protocol was utilized to create the RAD54 sensor.

The absorption spectra of antibody conjugated silver colloids was characterized by a further red shift (6nm) and surface Plasmon dampening as observed in Figure 36.

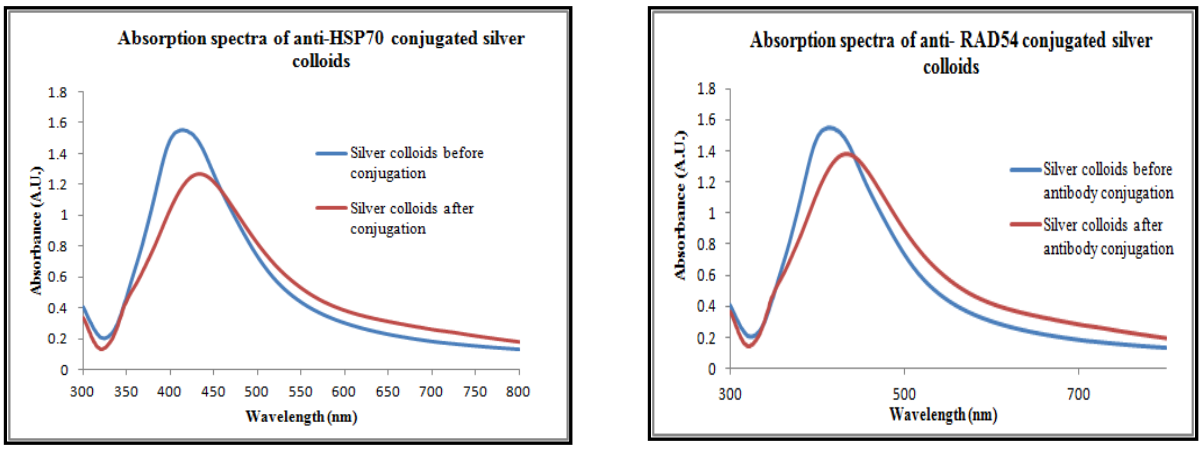

Figure 36: Comparison of Absorbance Spectrum of Silver Colloids before and after antibody conjugation (anti-Hsp70) conjugation (left) and Silver Colloids before and after antibody conjugation (anti-Hsp70) conjugation (right)

Anti-RAD54 antibody conjugation to linker self- assembled silver colloids also exhibited a red shift and plasmon dampening in their UV-Visible spectra as seen in anti-Hsp70 conjugated silver colloids (see Figure 36). The SERS spectra of the antibody conjugated silver colloids match well with the antibody (matching at 1177 cm^{-1} and 1060 cm^{-1}) as shown in Figure 35. Characteristic peaks at 1300 cm^{-1} are in the immunosensor corresponds to the self- assembled linker MMT. The peaks at 1650 cm^{-1} and 1560 cm^{-1} in SERS spectra of immunosensor correspond to the amide I and amide II band. These bands are missing in the spectra of anti-Hsp70 physisorbed onto silver colloids, thus providing positive signs of successful conjugation of protein with silver by formation of amide bond.

Binding of Antigen (Hsp70 and RAD54 respectively) to Antibody Conjugated (anti- Hsp70 and anti-RAD54 for Hsp70 and RAD54 sensor respectively) and Linker Self-Assembled Silver Colloids:

Antibody conjugated silver colloids were masked from nonspecific physical adsorption by using BSA before exposure to antigen (Hsp70; 20 ng/ml). The whole SERS sensor was characterized by Surface enhanced Raman spectroscopy (Figure 35).

The SERS spectra of antibody conjugated silver colloids after antigen interaction lost almost the entire characteristic vibrational fingerprint associated with the antibody. This could be due to a possible interaction of this complex (antibody conjugated silver colloids) with the antigen. Strong peaks corresponding to antigens were observed at 1558 cm^{-1}, 1393 cm^{-1}, 1132 cm^{-1}, 1007 cm^{-1} and 853cm^{-1}. The intensity of the vibrational bands of the antigen on interaction with immunosensor are much less in comparison to their intensity in the physisorbed state; thus showing the distance effect of the antigen and antibody. Since the vibrational spectra (SERS spectra of Hsp70 and RAD54 physisorbed onto silver colloids exhibited same spectra (Figure 37); we observed that SERS spectra of Hsp70 sensor interaction with Hsp70 antigen and corresponding spectra of RAD54 sensor interaction with RAD54 exhibited same peaks (Figure 38).

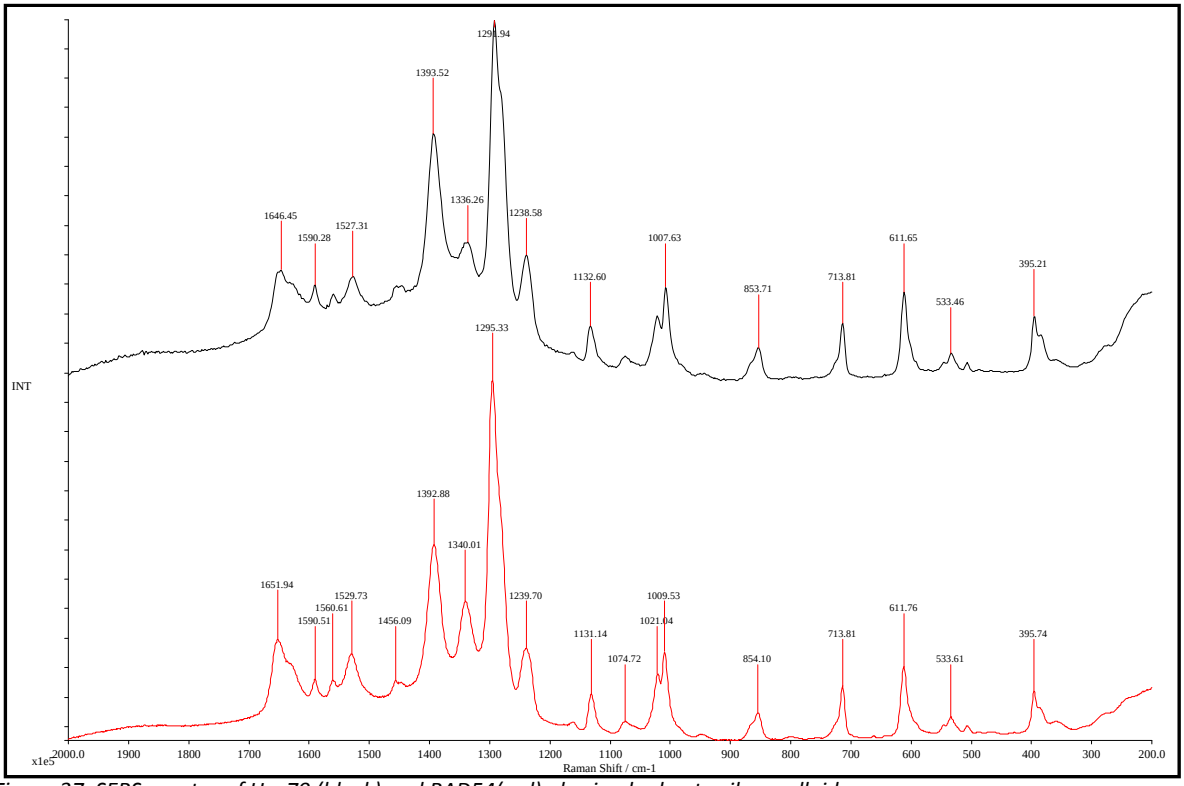

Figure 37. SERS spectra of Hsp70 (black) and RAD54(red) physisorbed onto silver colloids

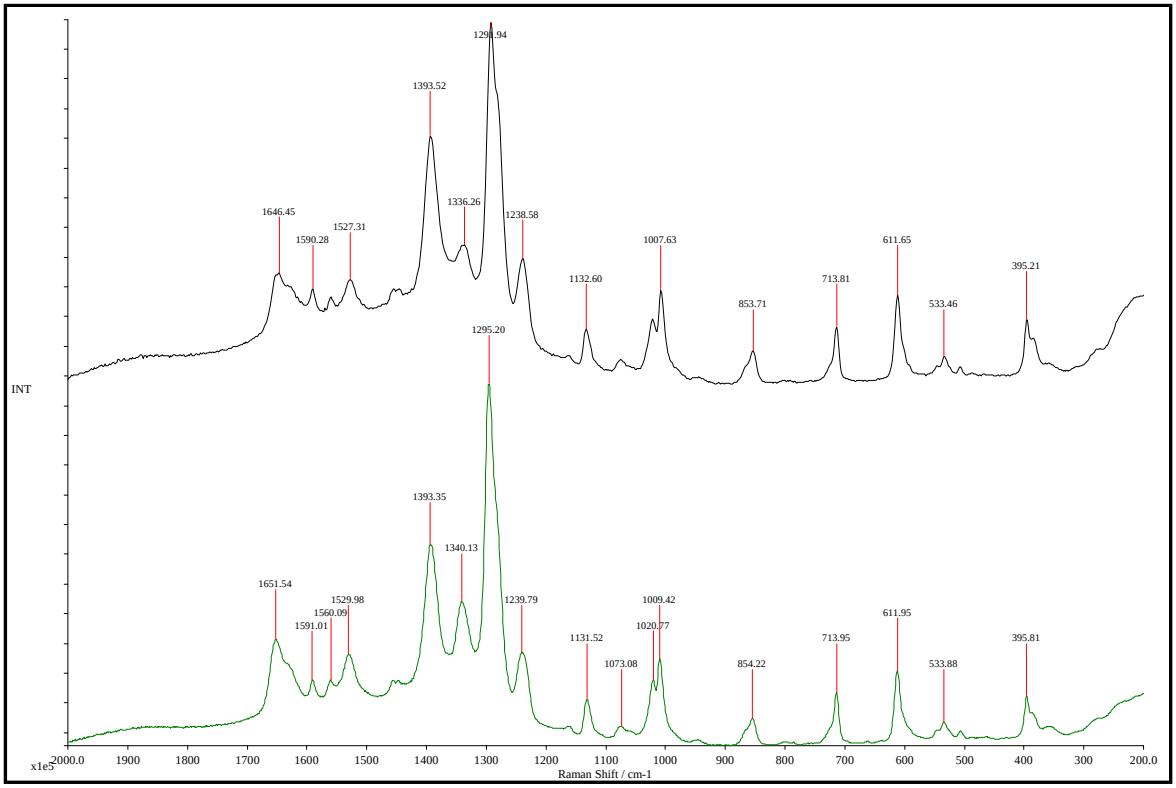

Figure 38. SERS spectra of Hsp70 immunosensor interaction with Hsp70 (2.5 ng/ ml; black) RAD54 immunosensor interaction with RAD54 antigen (2.5 ng/ml; green)

2.3.4. Comparative toxicity and uptake study of two types of AgNPs; citrate capped (Ag_{cit}) and SDS stabilized (Ag_{SDS})

Two types of AgNPs; Ag_{cit} (citrate capped Silver nanoparticles) and Ag_{SDS} (SDS stabilized silver nanoparticles) were tested for their biocompatibility (toxicity study) and internalization potential (uptake study) inside yeast cells, which are being used as a surrogate organism in our study, to choose the best material for our application.

A. Toxicity study

A growth inhibition study using UV-Vis spectrophotometer to test the toxicity effect of AgNPs, Ag_{SDS} and Ag_{cit} on growth of yeast cells was done. After synthesis of the two types of AgNPs they were centrifuged to separate NPs from vehicle solution (the liquid in which NPs are suspended), incubated with fixed number of cells (inoculum) for 12 hours under optimum growing conditions and absorbance at 600nm (OD600) measured. The final concentration (OD_{600}) was compared for negative control (no AgNPs, only media), vehicle controls (only the suspending liquid) and the experimental samples (3 doses of lyophilized AgNPs) (Figure 39).

B. Uptake study

Roughly 106 NPs/cell were added to yeast cells and incubated under mixing conditions for 12 hours followed by their washing to get rid of free AgNPs (Ag_{cit} and Ag_{SDS}). Samples were prepared to study their distribution on the yeast surface (SEM analysis) and the number of NPs being adsorbed and internalized (uptake analysis by UV-Vis spectrophotometer.

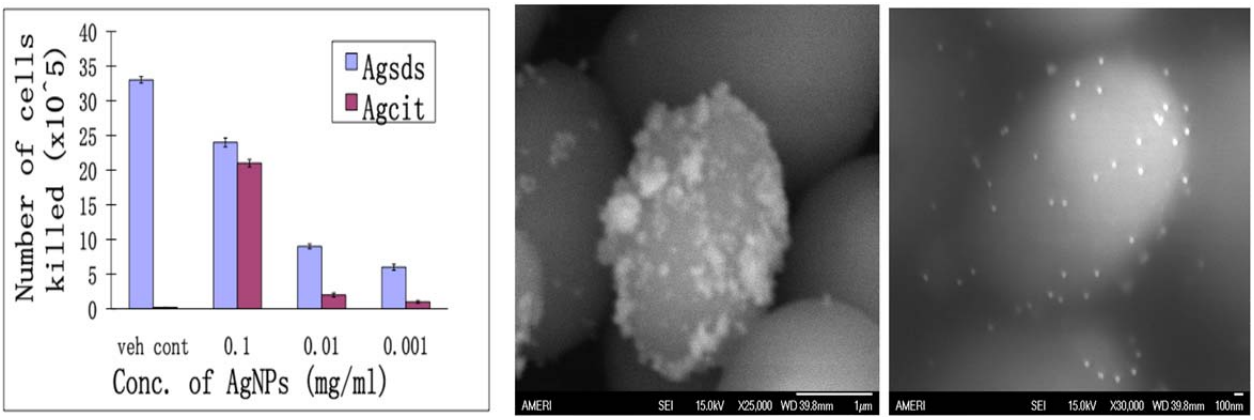

Figure 39: Toxicity and uptake study of two types of AgNPs; Ag_{SDS} and Ag_{cit} left) Toxicity of vehicle controls and lyophilized AgNPs (3 doses) normalized to negative control; right) surface distribution of Ag_{SDS} A) and Ag_{cit} b) on yeast cell.

A SERS effective concentration (0.1 mg/ml) of lypholized Agcit and Agsds killed 15% and 18% of the yeast cells under investigation (LC_{15} and LC_{18} values) respectively. The vehicle control of Agsds was found to be highly toxic as residues of reactants used (primarily SDS) might still be present due to incomplete reaction resulting in toxicity. The Vehicle control of Agcit was found to be non-toxic. From SEM images we observed that Ag_{SDS} formed agglomerate on yeast cell surface as compared to Agcit which was uniformly distributed as individual NPs. From the UV-Vis study we observed that Ag_{SDS} uptake in yeast

was roughly twice that of Ag_{cit} (3000 Vs 1400) (Figure 39). Our quantitative study is supported by the literture available on mammalian cells which are 4-5 times larger than yeast cells (15-20 micron Vs 4-6 micron) and hence is the expected uptake potential of metallic NPs (6000 Vs 1400-3000 NPs/cell). (Chitrani et al., 2006). The quantitative uptake study of the AgNPs using ICP-MS is in progress and is not reported here.

SDS coating around AgNPs might be the plausible reason for higher toxicity and uptake of Agsds into the yeast cells. SDS is a strong anionic detergent that interacts with lipids and proteins on cell surface increasing cell permeability or even rupturing if used in higher concentration (e.g.; SDS PAGE). The effect of SDS stabilized AgNPs contributing to toxicity on microbes; bacteria and yeast has been reported (Panacek et al., 2009, Kvitek et al., 2008, Hrenovic et al., 2007)

From the above study we concluded that citrate reduced silver Nanoparticles (Agcit) is a better SERS substrate over Ag_{SDS} and AuNPs and was thus used for fabrication of SERS sensor to detect stress proteins specifically in cell lysate (extracellular) and intact cells (intracellular).

Stress protein (Heat Shock Protein 70 and RAD54) quantification from yeast cell lysates:

Dose response curve for both Hsp70 and RAD54 sensor with their corresponding antigens were created as seen in Figure 40.

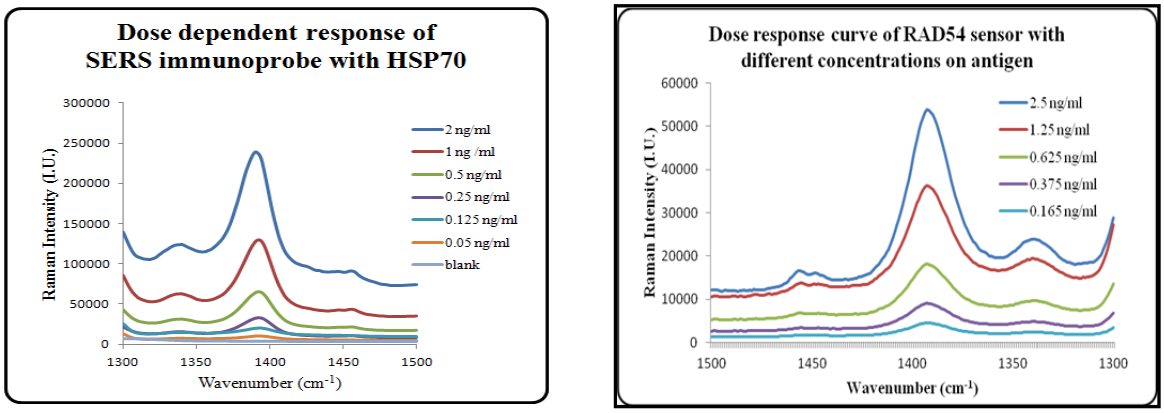

Figure 40. Dose dependent response of Hsp70 sensor and RAD54 sensor with different concentrations of Hsp70 (2ng/ml- 0.05 ng/ml) (left) and RAD54 (2.5 ng/ml - 0.165 ng/ml) (right) respectively

The Hsp70 and RAD54 SERS sensors provided a linear relationship with the increasing concentrations of antigens of Hsp70 (2ng/ml- 0.05 ng/ml) and RAD54 (2.5 ng/ml - 0.165 ng/ml) (R^2=0.99 for both sensors) (Fig. 41 and Fig. 42 respectively). These ranges of protein were found to be expressed in yeast measured using ELISA. Specificity check of the sensors with known strong raman reporters such as Rhodamine 6G, Cysteine and Glycine was conducted. No peaks associated with the reporters were found when they were allowed to interact with the antigen and the reporters.

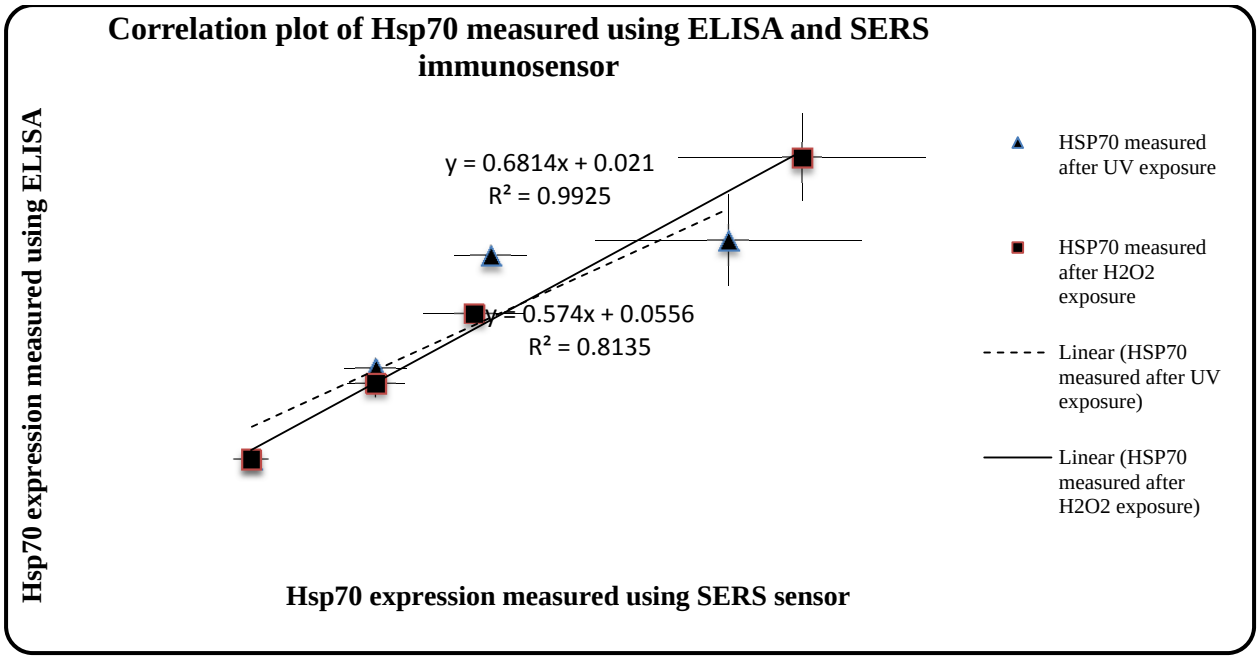

Figure 41. Correlation plot of Hsp70 measured using ELISA and SERS immunosensor

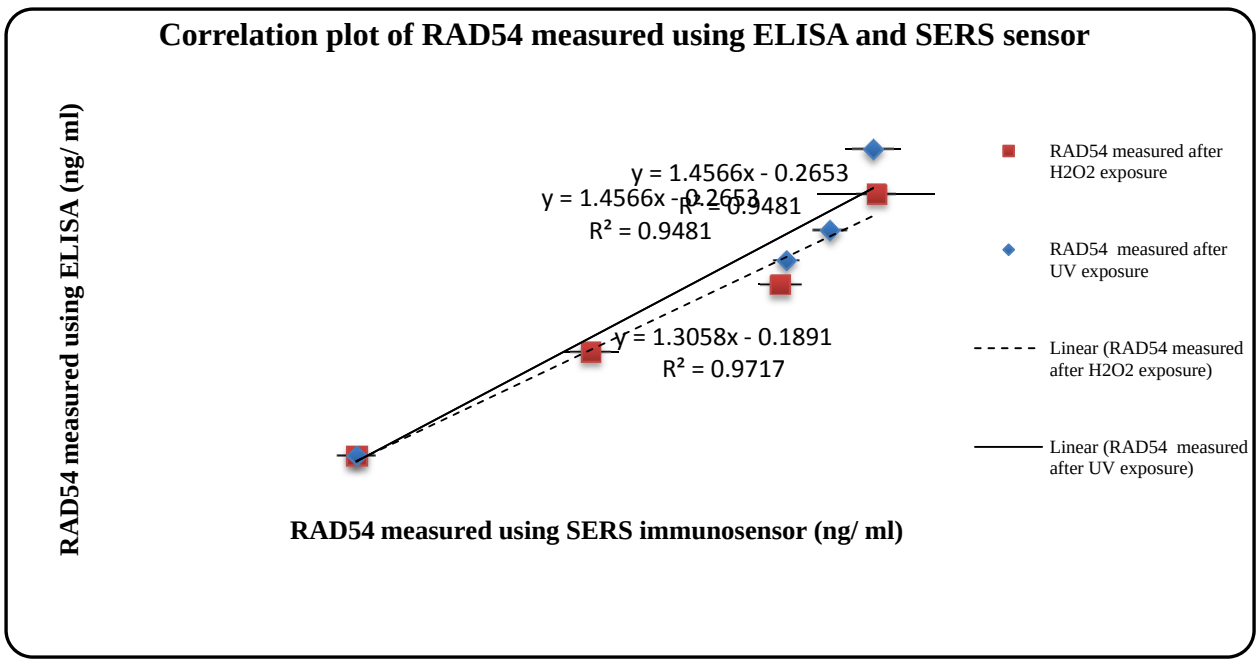

Figure 42. Correlation plot of Hsp70 measured using ELISA and SERS immunosensor

Thus we were successfully able to prepare Hsp70 and RAD54 sensors that could specifically detect the antigens in yeast cell lysates exposed to different levels of stressors (UV: low, medium and high wavelength and H_2O_2: 5,50 and 500 mM respectively.

2.3.5. Efficient delivery of SERS sensor for intracellular detection of stress:

After successful detection of stress levels in cell lysate we focused on optimization of SERS substrate for intracellular detection to develop the whole cell sensor.
For intracellular detection the efficient delivery of the SERS sensor in yeast cells to reach the stress markers (Hsp70 and RAD54) distributed ubiquitously inside the cell, is a pre-requisite. The efficient delivery in cytoplasm and organelles in turn depends on three limiting steps:

1. Delivery of sensor across the membranes. (Internalization)
2. Entrapment/compartmentalization in endosomes
3. Transport through crowded cytoplasm.

Three possible delivery techniques; Passive diffusion, facilitated delivery and active physical delivery were studied to determine the best delivery method for SERS sensor.

A) Passive diffusion

Bare silver Nanoparticles (AgNPs without any molecule conjugated to its surface) were incubated with yeast cells (105 NPs/cell) for 12 hours under mixing conditions. Free NPs were then washed and cell pellet was processed for ultra-thin sectioning (50-100 nm). The sections were then analyzed using TEM.

B) Facilitated delivery using cell permeability peptide (CPP) TATHA

Anti-biotin antibody was conjugated to silver Nanoparticles using a MMT linker following carbodiimide chemistry. To the anti-biotin decorated NPs, biotinylated TAT-HA2 (fusogenic CPP) was conjugated followed by PEG coating. The conjugation of TATHA2 to AgNPs was confirmed by Raman signature. The NPs were then incubated with yeast cells under mixing conditions for 2 hours. The samples were then sectioned and analyzed by TEM as stated above (Figure 43).

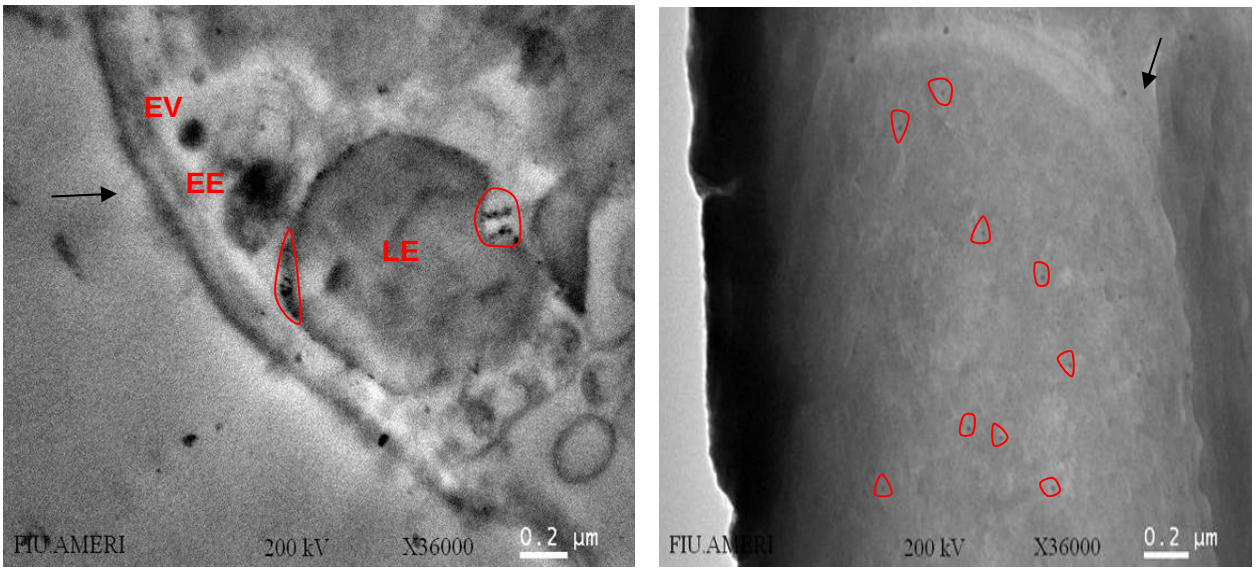

Figure 43: In Situ TEM images of ultra-thin yeast sections after left) passive and right) facilitated delivery of AgNPs. Circles enclose the NPs, arrow indicate the cell boundary. Different stages in the pathway of endycotosed AgNPs after passive diffusion are labeled as, endocytotic vesicle (EV), early endosomes (EE) and late endosomes (LE).

Silver NPs were found entrapped in endosomes after 12 hours of passive delivery/diffusion while the TATHA2 facilitated the uniform dispersion of AgNPs inside yeast.

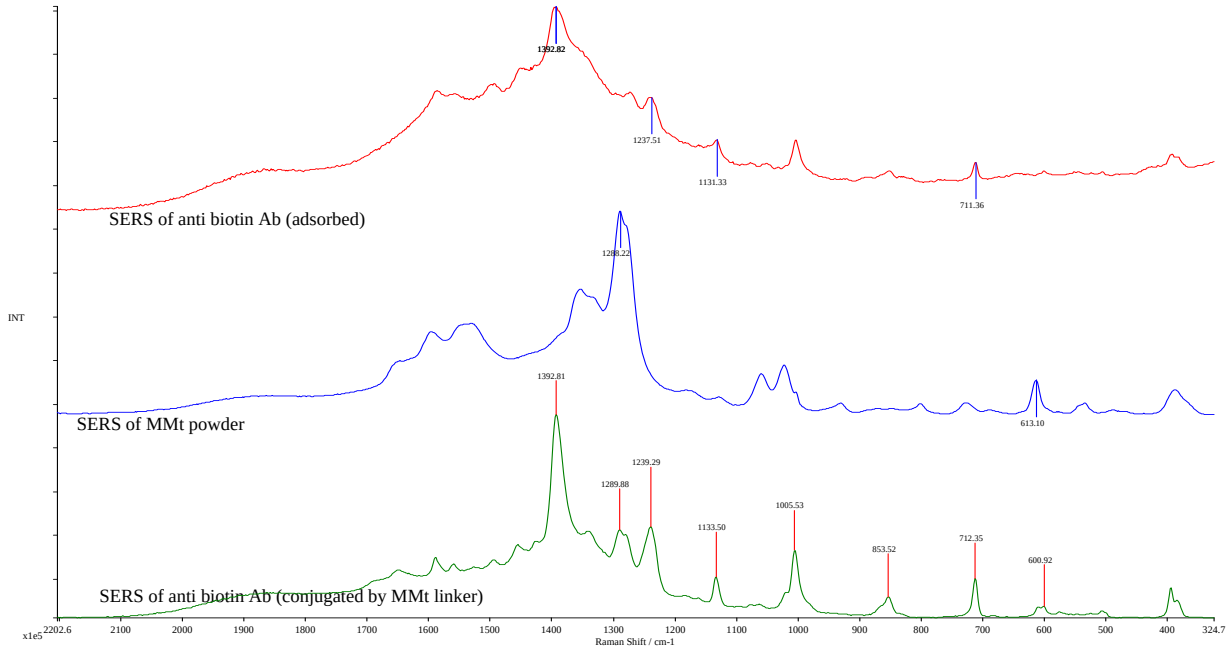

Figure 44: SERS signature of adsorbed MMT linker and Ab (top two) and Ab conjugated through MMT linker (bottom). Bands at 1392 and 712 (tryptophan), 1005 and 600 (Phenyl alanine), 1133, 853 (Tyrosine) correspond to three Raman active aromatic amino acids characteristic to peptide.

C) Active delivery by Electroporation

Low voltage electric field was applied to deliver the bare AgNPs. Different parameters (dose, duration and number of electric pulses) were tried to optimize active physical delivery in terms of little/no toxicity. 106 AgNPs/cell were incubated and electroporated under cold conditions. The control (cells without AgNPs and cells with AgNPs but without electroporation) and experimental samples (cells with AgNPs and electroporation) were tested for toxicity effect of electroporation employing qualitative and quantitative methods; colonogenic assay, SEM and vital staining (Figures 45).

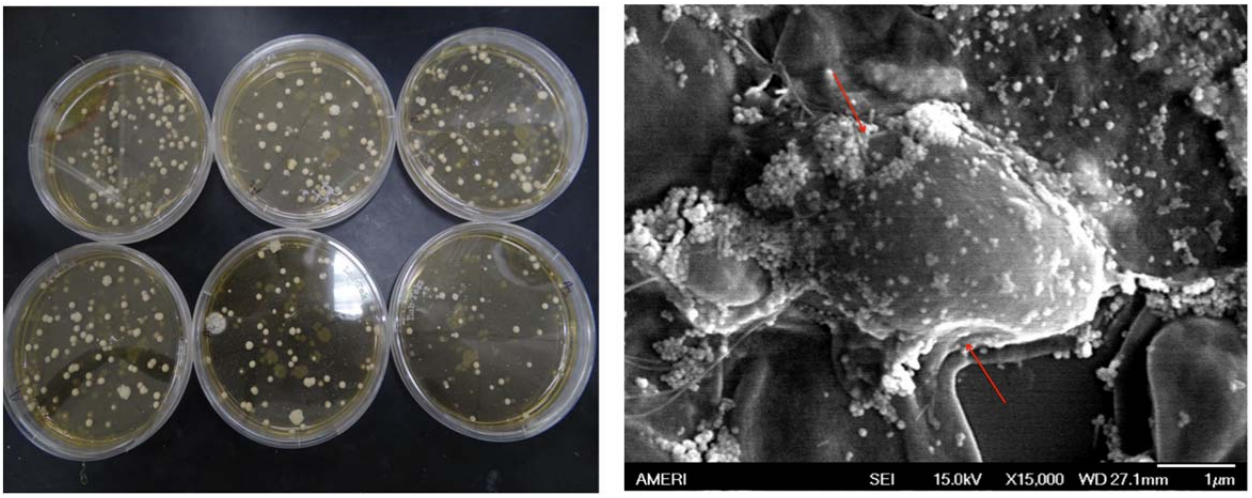

Figure 45: Cytotoxicity effect of electroporation (0.5 V/cm electric field) with different pulse duration left) Colonogenic assay; control, 1ms, 4ms right) SEM image of cell after 0.5 V/cm for 4ms showing damage to the yeast surface (indicated by arrow).

The low dose of electric field strength (0.5 V/cm) proved to be toxic to the yeast cells.

After conducting three uptake techniques for AgNPs delivery we conclude that facilitated delivery by conjugating TATHA2 CPP and PEG coating is the best choice for efficient delivery of SERS substrate to develop whole cell sensor. Besides being non-toxic (Wadia, 2004) this smart combination can confer all three desired properties for an efficient delivery. TAT moiety can increase internalization through macropinoctosis (Wadia, 2004), pH sensitive HA2 can rupture release particles from endosome (Wadia et al., 2007) and PEG coating can facilitate transport in crowded cytoplasm (Suh et al., 2007) trafficking them to organelles. Electroporation on the other hand is not only toxic but is also reported to elevate level of stress proteins (Tupaj et al., 2011) which might interfere with their expression levels in response to stress in our study; H_2O_2 and U.V.

Problems encountered:

The SERS sensor formed aggregates, which had little or no uptake in yeast cells.
RAD54 and Hsp70 could not be detected label- free using the aforementioned technique due to great similarity in their spectra.

Possible solutions to problem:

1. Using alternate cross- linking agents such as Sulfo- NHS that would help provide negative groups and hence enhance stability of the intermediate for antibody conjugation.
2. Change molar ratio of EDC: Sulfo NHS and amount added to linker- colloids.
3. Change initial antibody concentration
4. PEGylation to increase stability of the colloids
5. Label- based SERS detection of Hsp70 and RAD54

3. Key Research Accomplishments

3.1. Cytogenetics Assays

- Completed IRB documentation to enable collection of human blood samples and subsequent approval
- Recruited successfully 53 subjects to participate in the study
- Established the parameters for culturing human lymphocytes
- Finalized the process for defining dose response of lymphocytes to H_2O_2
- Finalized the process for defining dose response of lymphocytes to UV
- Initiated and established protocols for the CA assay
- Initiated and established protocols for the MN assay
- Initiated and established protocols for the comet assay
- Identified chromosome aberrations at all exposure concentrations of H_2O_2 (5-80mM) and duration of UV exposure (5-30 minutes). Clear associations have been found with increasing numbers of aberrations and severity of aberrations with increasing H_2O_2 concentrations and UV exposure. H_2O_2 treatments produced more varied chromosomal aberrations than did UV exposure
- Established FISH protocols for various commercially available FISH probes in lymphocyte nuclei and chromosomes suitable for use in combination with the DNA damage assays should a greater sensitivity be required for comparisons to one or both biosensors
- Data has been generated for the MN assay for both H_2O_2 and UV treatments. Our data demonstrate that UV does not readily induce micronuclei formation and that UV exposure clearly reduces cell proliferation and apoptosis. For H_2O_2 we observe an increase in micronuclei formation with increasing concentration of the agent as well as observing a reduction in cell proliferation with treatment

3.2. EIST Based Biomarker Sensor For Oxidative DNA Damage Assessment

- Collected colorimetric testing data using digital camera and quantitatively analyzed colorimetric testing of standard 8-OHdG by ImageJ software
- Successfully obtained a 3-D intensity profile of standard 8-OHdG solution using ImageJ and Sigma plot software, providing a more quantitative view compared to the graph generated from the digital camera
- Collected and tested urine samples from healthy, non-smoking participants, and determined that urine sample pretreatment including filtration and dilution are required to establish a reliable calibration curve
- We tested the 8-OHdG in urine samples, and demonstrated the sensitivity to be about 10 ng/ml using raw urine samples. After a 10 fold dilution of raw urine sample using DI water, the sensitivity is significantly improved from 10 ng/ml up to 0.1 ng/ml. Urine samples diluted 10 fold can eliminate the background effect (other proteins, small molecules, etc), which, exist in itself to a large extent. Dilution was shown to provide more reliable and reproducible results
- Established a calibration testing curve of 8-OHdG in RPMI cell growth medium

- Successfully detected 8-OHdG in cell growth medium (RPMI) after exposure of cells (Lymphocytes) to UV
- Successfully detected 8-OHdG in cell growth medium (RPMI) after exposure of cells (Lymphocytes) to hydrogen peroxide (H_2O_2)
- Completed the surface characterization of CNT paper by SEM
- CNT paper electrode (working electrode) and silver/silver chloride electrode (reference electrode) have been successfully integrated to the paper strip based platform
- Tested the standard 8-OHdG solutions by using CNTs paper based electrochemical immunostrip with multiple detection design. And preliminary data showed that the detection limit can reach as low as 1 ng/ml. Sensitivity can be improved by reducing the sensing surface of working electrode in future. Continued work is required to get a more detail calibration testing curve for this part

3.3. SERS Based Gold Nanoparticle Whole-Cell Biosensor

- Prepared Hsp70 and RAD54 sensor for specific detection of Hsp70 and RAD54 in the range expressed by yeast cells.
- Measured levels of Hsp70 and RAD54 using SERS sensors and correlated with those obtained by ELISA from yeast cell lysates.

4. Reportable Outcomes

4.1. Cytogenetics

Journal Publications

Simpson JL, Preimplantation genetic diagnosis to improve pregnancy outcomes in subfertility. Best Pract Res Clin Obstet Gynaecol. 2012 26(6):805-15.

Simpson JL, Is Cell-Free Fetal DNA From Maternal Blood Finally Ready for Prime Time? Obstet & Gyne. (2012) 119, 5 883-885.

Wapner RJ, Martin, CL, Levy B, Ballif BC, Eng CM, Zachary JM, Savage, M, Platt LD, Saltzman D, Grobman, WA, Klugman S, Scholl T, Simpson JL, McCall K, Aggarwal VS, Bunke B, Naham O, Patel A, Lamb, AN, Thom EA, Beaudet AL, Ledbetter DH, Shaffer LG and Jackson L. Chromosomal Microarray Compared with Karyotyping for Prenatal Diagnosis. N Engl J Med. (2012) In press.

Mouawia H, Saker A, Jais J-P, Benachi A, Bussieres L, Lacour B, Bonnefont J-P, Frydman R, Simpson JL, Paterlini-Brechot P. Circulating trophoblastic cells provide genetic diagnosis in 63 fetuses at risk for cystic fibrosis or spinal muscular atrophy. Reprod. BioMed Online (2012). In press.

Millan N, Lau P, Hann M, Ioannou D, Hoffman D, Maxson W, Ory S, Tempest HG. Hierarchical radial and polar organization of chromosomes in human sperm. Revision under review, submitted to Chromosome Research.

4.2. EIST Based Biomarker Sensor For Oxidative DNA Damage Assessment

Journal Publications

X. Zhu, E. Hondroulis, C.-Z. Li, Biosensing Approach for Rapid Genotoxicity and Cytotoxicity Assay upon Toxic Exposure, Small (IF 8.407), revision under review

P. Shah, X. Zhu, Development of Paper-based Analytical Kit for Point of Care Testing, Expert Review of Molecular Diagnostics (IF 4.859). In press.

C.-Z. Li, K. Vandernberg, S. Prabhulkar, X. Zhu, L. Schneper, K. Methee, C.J. Rosser, E. Almeide, Paper Based Point-of-Care Testing Disc for Multiplex Whole Cell Bacteria Analysis, Biosensors and Bioelectroncs (IF 5.483), 2011, 26, 4342-4348.

Conference Presentations

Xuena Zhu, Pratik Shah, Dr. Chenzhong Li, "Paper based Point of Care testing sensor for DNA oxidative damage biomarker detection", Pittcon 2012, March 11-15, Orlando, Florida.

C.-Z. Li, “Paper Based Point-of-Care Testing Sensors for Quantitative Analysis of Biomarkers and Bacterial Cells”, April 16th, 2012, Future Diagnostics Symposium, Irvin, CA.

C.-Z Li, “Low Cost Paper Based Point of Care Testing Sensors for Bacterial Cells and Biomarker Detection”, 2012 World Congress on Medical Physics and Biomedical Engineering, May 27, 2012, Beijing, China.

C.-Z. Li, “Biosensors for Rapid Analysis of Nanotoxic Kinetics”, September 6th, 2012, 6th Nanotoxicology conference, Beijing, China.

X. Zhu, C-Z. Li, “Paper based sensor for DNA damage biomarker detection”, Sep 28-29, NanoFlorida 2012, Tampa, Florida.

C.Z. Li, “Biosensing Device for Toxicity Assessment of Nanomaterial”, 2012 Nanoflorida, September 28-29, Tampa, FL.

C.-Z. Li, Biotronics 2012, October 17th, Guangju, South Korea.

4.3. SERS Based Gold Nanoparticle Whole-Cell Biosensor

Oral presentation in the NanoBio Conference (2012) on the topic “Sensitive and Specific Detection of Heat Shock 70 Stress Proteins using Label- free Immuno SERS Sensor”. Authors: Supriya Srinivasan, Joshy F. John, Vinay Bhardwaj, and Anthony J. McGoron.

5. Conclusions

5.1. Cytogenetic Assays

To date, we have completed dose response experiments for both UV and H_2O_2 for all three assays (CA, MN and comet). Our data clearly show that lower levels of UV exposure and H_2O_2 concentration are capable of eliciting DNA damage in the MN and comet assay, whereas an increased duration of exposure to UV and H_2O_2 concentration is required for the CA assay. Increasing concentration and duration of exposure of lymphocytes to UV and H_2O_2 respectively has resulted in a reduction in cell proliferation and an increase in cell death (apoptosis), which has been carefully monitored by assessing the mitotic index (CA assay), the CBPI (MN assay) and observation of apoptotic cells in the comet assay. Reduction in cell proliferation and increase in apoptosis at the various tested concentrations and exposure were utilized in calculating the maximal dose of the genotoxic agent to ensure that a high proportion of cells were still viable and capable of undergoing cell division. For the CA assay we have demonstrated that H_2O_2 treatment induces more different types of structural chromosomal rearrangements than that of UV in which we also observe chromosomal aberrations. The number of aberrations observed and an increase in severity of the chromosomal damage observed for both UV and H_2O_2 exposure was correlated with increasing concentration and exposure of the genotoxic agents. We have observed that the formation of micronuclei can be induced after H_2O_2 treatment and an increase in number is observed with increasing concentration. However, UV exposure does not induce the formation of micronuclei with extremely low levels that do not alter with increasing exposure to UV. Both agents UV and H_2O_2 have been shown to be capable to induce single and double-stranded breaks in DNA as determined by the comet assay. The comet assay has produced clear data that demonstrates increasing exposure or concentration of our agents is correlated with increasing levels of DNA associated with single and/or double-stranded DNA breaks.

5.1.1. Future Plan

- Continue and finalize the CA assay analysis of H_2O_2 and UV treated lymphocytes
- Finalize the MN assay in H_2O_2 treated lymphocytes
- Process and analyze the last few samples of UV and H_2O_2 treated lymphocytes for the comet assay
- Combine FISH with the CA, MN assay and comet assay if it is deemed necessary to increase the sensitivity of the cytogenetic assays to be comparable to the biosensors
- Perform comparisons between the results obtained from the cytogenetic assays and those results of the biosensors
- Extend assay validation by use of other toxicants designated by DOD if required

5.2. EIST Based Biomarker Sensor For Oxidative DNA Damage Assessment

We have successfully established a calibration method for quantitative analysis of 8-OHdG colorimetric testing in standard solution, diluted urine and cell culture medium.

We also successfully integrated the Carbon nanotube (CNT) paper electrode to the paper strip based platform, and tested the 8-OHdG concentrations by traditional colorimetric method as well as electrochemical method.

In summary, the combined EIST provide a point of care testing method for rapid risk assessment of unspecified toxin with high sensitivity, specificity, speed of performance and the advantages of simplicity.

5.2.1. Future Plan

- Collect more urine samples followed the IRB protocol and start to try to test the clinical sample by electrochemical method
- Improve the sensitivity of the integrated paper strip by reducing the sensing surface of working electrode.
- Establish the correlation of experimental data based on both optical and electrochemical measurements in order to derive a realizable calibration curve for 8-OHdG detection.
- Validate of the sensing system by comparing our testing results to those of laboratory standard methods, namely COMET or HPLC-MS.
- In future, the portable potential stat will connect to smart phone via blue tooth technology and data can be got conveniently and fast.

5.3. SERS Based Gold Nanoparticle Whole-Cell Biosensor

In conclusion, we have demonstrated the proof-of-concept that silver, and possibly gold, are suitable SERS substrates for selective and specific detection of Hsp70 and RAD54 proteins from yeast exposed to environmental stress, but have not yet been able to load sufficient quantities of the SERS sensors into the yeast cells to measure the proteins intracellularly.

5.3.1. Future Plan

- Sort the aggregation issue and measure Hsp70 and RAD54 proteins intracellularly using the sensors mentioned above.

5.4. General Conclusion

Currently there is no practical or rapid method to monitor exposure to genotoxic agents of unknown nature. The current approach for assessing genome toxicity relies principally on scoring chromosomal abnormalities. These measures of genotoxicity are currently only possible through laborious cytogenetic evaluations requiring dedicated lab personnel with extensive training. We have made significant progress toward development of two prototype biosensors to detect non-specific DNA damage: (i) EIST biosensor measuring reactive oxygen species specifically 8-OHdG; and (ii) SERS biosensor measuring several stress proteins.

These three seemingly disparate projects detailed in this report will culminate in a common goal to compare the sensitivity and specificity of the ability of these two prototype biosensors to detect genotoxic damage, as determined by gold-standard cytogenetic assays. Success of one or both of the biosensor devices compared to that of standard genotoxic assays will be established using standard statistical methodology, and judged by the ability of the devices to achieve equal or increased sensitivity of the gold-standard assays. Specifically, do the biosensors produce a measurable response at the same genotoxic concentration as in cytogenetic assays, and do the biosensor devices produce a dose related response as seen in the cytogenetic assays? We will then be able to determine whether one or more biosensor has the ability to detect the presence of toxicants more rapidly and sensitively than conventional cytogenetics assays. If so, we will then focus future efforts toward assuring "rugged" devices suitable to be worn or utilized in military theatre. This will require experimentation in collaboration with TATRC beyond the current time span of this contract.

6. References

Aroca R. Surface-Enhanced Vibrational Spectroscopy, John Wiley & Sons Ltd., Chichester, 2006.

Devika C., Ghazani A.A. Determining the size and shape dependence of gold nanoparticles uptake in mammalian cells Nano Letters 2006 vol., No.4 662-668.

Glei M., Hovhannisvan G., Pool-Zobel B.L. Use of Comet-FISH in the Study of DNA Damage and Repair: Review. Mutat. Res. 681, 33-43, 2009.

Hrenovic J, Ivankovic T. Toxicity of anionic and Cationic surfactants to Acinetobacter junii in pure culture. Central European Journal of Biology 2007; 2:337-48.

Kang K.A., Zhang R., Lee K.H., Chae S., Kim B.J., Kwak Y.S., Park J.W., Lee N.H., and Hyun J.W. "Protective effect of triphlorethol-A from Ecklonia cava against ionizing radiation in vitro", J. Radiat. Res., 47, 61–8, 2006.

Kasai H., Nishimura S. Hydroxylation of deoxyguanosine at the C-8 position by ascorbic acid and other reducing agents. Nucleic Acids Res., 12, 2137-2145, 1984.

Kuhn J.F., Hoerth P., Hoehn S.T., Preckel T. and Tomer K.B. Proteomics study of anthrax lethal toxin-treated murine macrophages. Electrophoresis. 27, 1584–97, 2006.

Kvitek L, Panacek A. Effect of surfactants and polymers on stability and antibacterial activity of silver Nanoparticles. Journal of physical Chemistry Part C 2008; 112:5825-34.

Lee P.C. and Meisel D. Adsorption and surface enhanced Raman of dyes on silver and gold sols. J. Phy. Chem. 86 (1982) 3391-95.

Li C-Z., Vandernberg K., Prabhulkar S., Zhu X., Schneper L., Mathee K., Rosser C.J., Almeide E. Paper based point-of-care testing disc for multiplex whole cell bacteria analysis, Biosensors and Bioelectroncs. 26, 4342-4348, 2011.

Li H., Sun J, and Cullum B. M. J. Label-Free Detection of Proteins Using SERS-Based Immuno-Nanosensors. Nanobiotechnology. 2006, 2, 17- 21.

Liu C., Jia Q., Yang C., Qiao R., Jing L., Wang L., Xu C., Gao M., Anal Chem 83 (17), 6778-84 2011.

Nie S, Emory S.R. Probing Single Molecules and Single Nanoparticles by Surface-Enhanced Raman Scattering. Science. (1997), 275, 1102-1106.

Panacek A, Kolar M. Antifungal activity of Silver Nanoparticles against Candida spp. Biomaterials 30 (2009) 6333-6340.

Sari-Minodier I., Orsiere T., Auquier P., Martin F., Botta A. Cytogenetic Monitoring By Use Of The Micronucleus Assay Among Hospital Workers Exposed To Low Doses Of Ionizing Radiation. Mutat. Res. 618, 111-121, 2007.

Sperati A., Abeni D.D., Tagesson C., Forastiere F., Miceli M., Axelson O. Exposure to indoor background radiation and urinary concentrations of 8-hydroxydeoxyguanosine, a marker of oxidative DNA damage. Environ. Health Perspect. 107, 213–215, 1999.

Suh J. PEGylation of nanoparticles improve their cytoplasmic transport. International Journal of Nanomedicine (2007) 2(4) 735-741.

Tupaj M.H. Osteoblastic differentiation and stress response of human mesenchymal stem cells exposed to alternating current electric fields. Biomed Eng online (2011) 10:9.

Wadia J.S., Transducible TAT-HA fusogenic peptide enhance escape of TAT-fusion proteins after lipid raft macropinocytosis. Nature Med (2004) 310.

Wang D., Li Y. Effective Octadecylamine System for Nanocrystal Synthesis. Inorg. Chem. 40, 5196-5202, 2011.